Earth-Science Reviews 258 (2024) 104946

Contents lists available at ScienceDirect

Earth-Science Reviews

journal homepage: www.elsevier.com/locate/earscirev

# Global hydroclimate perturbations during the Toarcian oceanic anoxic event

David B. Kemp [a,*], Zhong Han [b], Xiumian Hu [c], Wenhan Chen [b,d], Simin Jin [e], Kentaro Izumi [f], Qing Yan [g,h], Viktória Baranyi [i], Xin Jin [b], Jacopo Dal Corso [j], Yuzhu Ge [b]

[a] State Key Laboratory for Biogeology and Environmental Geology and Hubei Key Laboratory of Critical Zone Evolution, School of Earth Sciences, China University of Geosciences (Wuhan), Wuhan 430074, China
[b] State Key Laboratory of Oil and Gas Reservoir Geology and Exploitation & Institute of Sedimentary Geology, Chengdu University of Technology, Chengdu 610059, China
[c] State Key Laboratory of Mineral Deposit Research, School of Earth Sciences and Engineering, Nanjing University, Nanjing 210023, China
[d] International Center for Sedimentary Geochemistry and Biogeochemistry Research, Chengdu University of Technology, Chengdu 610059, China
[e] Department of Atmospheric Science, School of Environmental Studies, China University of Geoscience (Wuhan), Wuhan 430074, China
[f] Faculty & Graduate School of Education, Chiba University, 1-33 Yayoi-cho, Inage-ku, Chiba-shi, Chiba, Japan
[g] Nansen-Zhu International Research Centre, Institute of Atmospheric Physics, Chinese Academy of Sciences, Beijing 100029, China
[h] Key Laboratory of Meteorological Disaster/Collaborative Innovation Center on Forecast and Evaluation of Meteorological Disasters, Nanjing University of Information Science and Technology, Nanjing 210044, China
[i] Department of Geology, Croatian Geological Survey, Sachsova 2, 10000 Zagreb, Croatia
[j] State Key Laboratory for Biogeology and Environmental Geology, China University of Geosciences (Wuhan), Wuhan 430074, China

ARTICLE INFO

*Keywords:*
T-OAE
Hydrological cycle
Storms
Hyperthermal
Carbon release
Runoff

ABSTRACT

An intensification of the hydrological cycle is an expected consequence of global warming, and this will likely lead to spatially variable precipitation and drought extremes, and more intense tropical storms. Deep time hyperthermal events, characterised by large-scale carbon release and transient global warming, have the potential to provide insights into the nature and magnitude of hydroclimate changes in response to warming. The Toarcian oceanic anoxic event (T-OAE, or Jenkyns Event, ~183 Ma) was a severe hyperthermal, and is associated with evidence for marked changes in hydroclimate, including: intensified tropical cyclone activity, an increase in global chemical weathering rates, and elevated freshwater runoff and terrigenous sediment fluxes to basins. Nevertheless, key knowledge gaps exist regarding the scale, significance, distribution and interpretation of these changes. Here, we review the evidence for T-OAE hydroclimate changes based on published data from 109 sites. Although these sites are primarily concentrated in the northwest Tethys region, we show that evidence for T-OAE hydroclimate change was globally distributed, and that most sites (63 %) record evidence consistent with an intensification of hydrological cycling under hotter conditions likely characterised by weather/precipitation extremes. Evidence for enhanced storm activity is common; recorded at up to a third of sites from both low and middle latitudes. This evidence is consistent with climate model predictions of increased tropical cyclone intensity and a poleward shift in storm tracks under elevated atmospheric $CO_2$. Evidence for enhanced weathering and terrigenous fluxes is also common. This evidence, coupled with the evidence for increased storminess, may help explain increased turbidite deposition during the event recorded at some deep-water sites. Although affected by geographic and perhaps sedimentological biases, our findings underline how hydroclimate change was an inherent and perhaps defining characteristic of the T-OAE, potentially of equal paleoenvironmental significance to the seawater deoxygenation that originally defined the event.

## 1. Introduction

Understanding the responses and sensitivity of the global hydrological cycle to rising atmospheric $CO_2$ and temperature at the present day is a key challenge, and one of social and economic importance. Warming, and consequent increase in atmospheric water storage,

* Corresponding author.
*E-mail address:* davidkemp@cug.edu.cn (D.B. Kemp).

https://doi.org/10.1016/j.earscirev.2024.104946
Received 1 July 2024; Received in revised form 23 September 2024; Accepted 30 September 2024
Available online 5 October 2024

is predicted to lead to large-scale but spatially variable changes in hydroclimate, such as increases in storm intensity, extreme precipitation events and fluvial sediment loading in some areas, but aridification in other areas (e.g., Trenberth et al., 2003; Hirabayashi et al., 2013; Knutson et al., 2020; Syvitski et al., 2022; IPCC, 2023). Observational data obtained over the last few decades suggest that such changes are already underway, with evidence for increases in the frequency of intense tropical storms in some regions, and elevated occurrences globally of precipitation and drought extremes (Emanuel, 2005; Elsner et al., 2008; Bhatia et al., 2019; Roddell and Li, 2023). However, modern observational datasets of hydroclimate change are limited by their relatively short duration. In particular, recognizing robust trends in storm activity over the last few decades has proven difficult (e.g., Landsea et al., 2006). Equally, determining the impact of Anthropogenic warming on weathering and runoff changes is difficult because fluvial sediment transport and storage processes typically operate on timescales of $>10^4$ years (Dosseto et al., 2015). Furthermore, quantifying the impact of warming on sediment fluxes to lakes and seas is difficult because human activities such as dam building mask these signals (Kemp et al., 2020a).

An understanding of how warming impacts hydroclimate can be gained by studying the geological record of ancient hyperthermal events. These events were characterised by geologically brief (<1 Myr) increases in global temperature and atmospheric $CO_2$, and thus have the potential to provide insights into the nature of hydroclimate responses to warming over relatively long ($10^3$ to $10^6$ yr) timescales and under different background climate states. Geochemical, paleontological and sedimentological evidence clearly indicates that changes in hydroclimate accompanied some of the most pronounced hyperthermal events of the Phanerozoic, including the Permian-Triassic mass extinction (~252 Ma, e.g., Sheldon, 2006; Algeo and Twitchett, 2010; Cao et al., 2019; Yang et al., 2023), the Carnian pluvial episode (~233 Ma, CPE, Simms and Ruffell, 1989; Dal Corso et al., 2024), the early Toarcian oceanic anoxic event (T-OAE, ~183 Ma, Cohen et al., 2004; Izumi et al., 2018), and the Paleocene-Eocene thermal maximum (PETM, ~55 Ma, Ravizza et al., 2001; John et al., 2008; Pujalte et al., 2015; Carmichael et al., 2017, 2018).

Of the above events, the T-OAE (or Jenkyns Event) exhibits some of the best and most geographically widespread evidence for hydroclimate change (see esp. Krencker et al., 2015; Han et al., 2018; Izumi et al., 2018; Kemp et al., 2020b; Baranyi et al., 2024). The T-OAE is marked in the sedimentary record by a pronounced negative carbon isotope excursion (NCIE) in marine and terrestrial reservoirs of carbon, indicating of a substantial release of $^{12}C$-enriched carbon into the biosphere (Hesselbo et al., 2000) (Fig. 1). The origin of this carbon is debated, and it may have been volcanogenic (i.e. from volcanic $CO_2$ outgassing, Pálfy and Smith, 2000), thermogenic (i.e. from igneous intrusion into organic-rich rocks, Svensen et al., 2007) and/or biogenic (e.g., from methane hydrates and/or soils, Hesselbo et al., 2000; Ruebsam et al., 2019). Proxy data indicate a likely doubling of atmospheric $CO_2$ (from ~500 ppm to ~1000 ppm) and a global seawater temperature rise of ~5 °C or more across the NCIE (Bailey et al., 2003; McElwain et al., 2005;

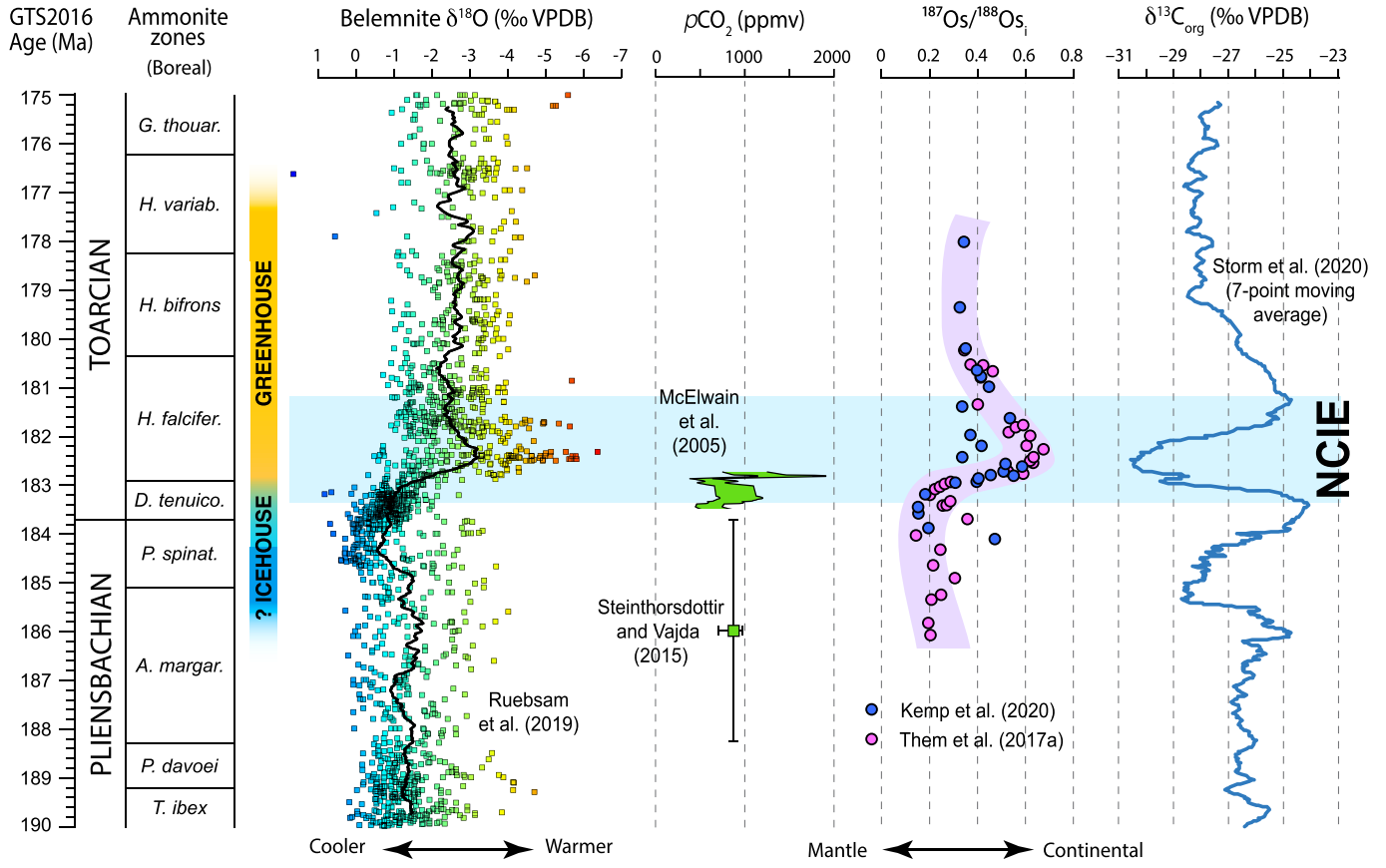


**Fig. 1.** Overview of paleoclimate data across the Toarcian oceanic anoxic event (T-OAE). Belemnite oxygen isotope ($\delta^{18}O$) data (a proxy for seawater temperature) and sea level curve are from Ruebsam et al. (2019). Atmospheric $CO_2$ data are from McElwain et al. (2005) and Steinthorsdottir and Vajda (2015). The representative carbon isotope curve (blue) is the organic carbon isotope ($\delta^{13}C_{org}$) record from the Mochras Farm (Llanbedr) borehole (Storm et al., 2020), and the negative carbon isotope excursion (NCIE) is labelled. Osmium isotope data are from Them et al. (2017a) and Kemp et al. (2020b). The positive shift in $^{187}Os/^{188}Os_i$ values across the NCIE indicates a global increase in continental-sourced (radiogenic) osmium relative to mantle-sourced (unradiogenic) osmium, and thus an increase in continental weathering. Figure modified from Kemp et al. (2020b). GTS2016 refers to Ogg et al. (2016). (For interpretation of the references to colour in this figure legend, the reader is referred to the web version of this article.)

Ruebsam et al., 2020a, 2020b; Nordt et al., 2022) (Fig. 1).

Although best known for its association with seawater deoxygenation (Jenkyns, 1988), T-OAE warming and atmospheric $CO_2$ rise were associated with a 200–500 % increase in silicate chemical weathering fluxes (Brazier et al., 2015; Them et al., 2017a; Kemp et al., 2020b) (Fig. 1). Coevally, enhanced terrigenous and nutrient fluxes to the oceans and reduced salinity of surface seawater have been linked to intensified erosion, fluvial sediment loads and runoff (e.g., Baranyi et al., 2016; Kemp et al., 2019; Remírez and Algeo, 2020). Abundant tempestite deposits are preserved in some low latitude (<30°) records of the event, suggesting an intensification of tropical cyclone activity during the event (Suan et al., 2013; Krencker et al., 2015; Han et al., 2018; Izumi et al., 2018; see also Yan et al., 2023). Overall, the T-OAE has the potential to provide insights into the operation of the

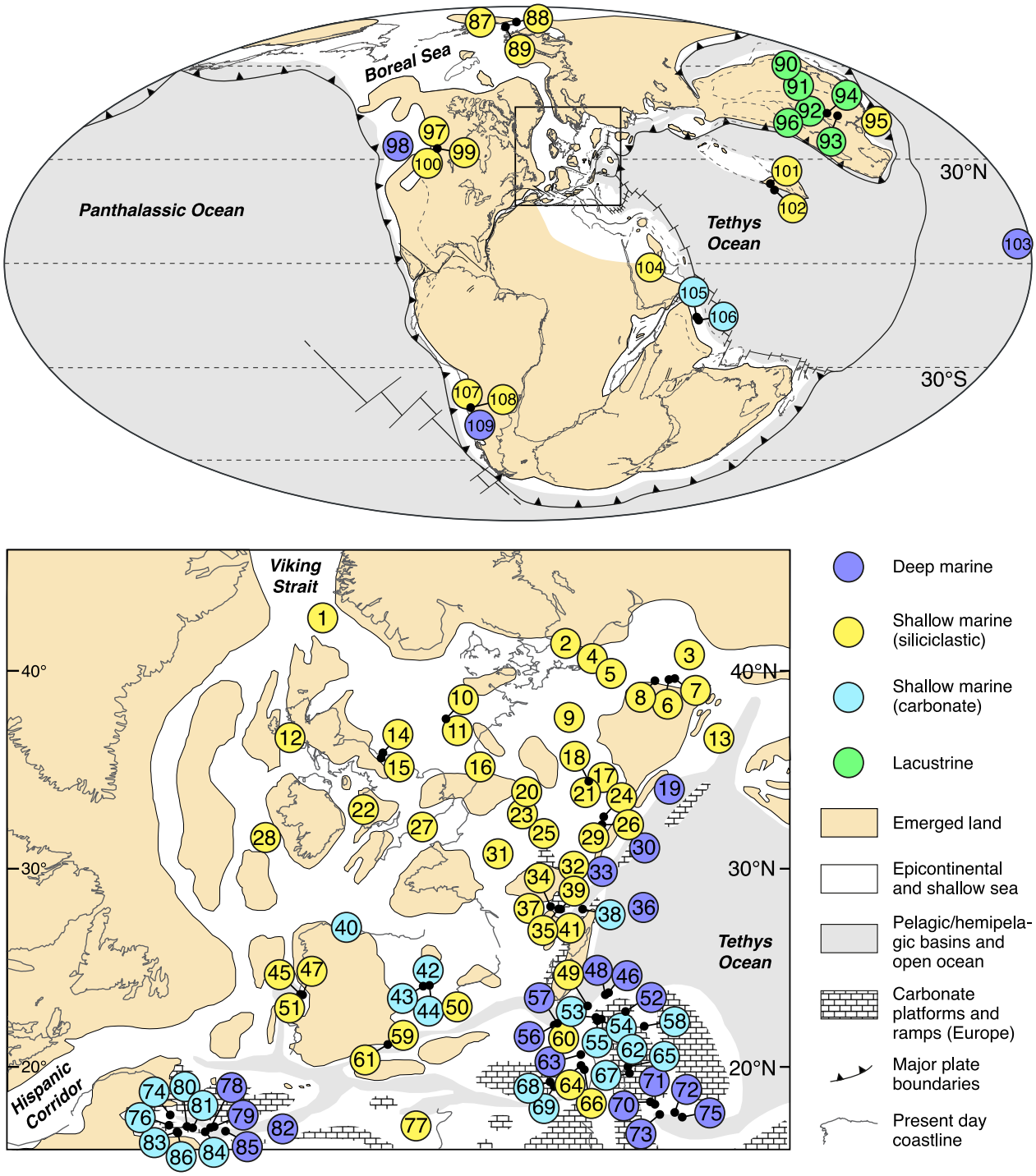


**Fig. 2.** Paleogeographic map of the early Toarcian (~183 Ma) with studied sites (109) shown. Sites are colour-coded based on depositional environment (lacustrine, shallow marine siliciclastic, shallow marine carbonate platform/ramp, and deep marine). Site names and hydroclimate data are in Table 1 (see Table S1 for fuller descriptions of the sites, including depositional environment/water depth interpretation and full descriptions of hydroclimate evidence). Sites are ordered by latitude and region (sites 1–86 = Europe/North Africa, sites 87–109 = rest of the world). Inset map shows the paleogeography of Europe and North Africa (area in black box on global map). Site locations are based on information provided in the source publications. Maps are from Kemp et al. (2022) and based on those in Müller et al. (2020).

hydrological cycle in response to extreme warming and $CO_2$ rise. Nevertheless, key knowledge gaps exist. For example, climate models predict that tropical cyclone tracks would shift poleward to subtropical regions under elevated $CO_2$ conditions (Korty et al., 2017; Studholme et al., 2021; Yan et al., 2023), but no systematic analysis of T-OAE tempestite distribution has been conducted that could test this. Similarly, the spatial pattern and significance of inferred changes in humidity/aridity during the T-OAE are unknown. Enhanced terrigenous sediment fluxes and decreased surface water salinity during the event may indeed have been linked to increased freshwater runoff under conditions of enhanced hydrological cycling, but the link between sediment yields and climate are complex (e.g., Syvitski et al., 2022), and decreased salinity has also been linked to freshwater fluxes from melting high-latitude ice sheets during T-OAE warming (e.g., Dera and Donnadieu, 2012; Ruebsam et al., 2019). In this study, we compile and review the evidence for hydroclimate and weather changes across the T-OAE in an effort to consolidate and improve understanding of how and where hydroclimate changed during the event.

## 2. Methods

We compiled evidence of potential hydroclimate change through the T-OAE from the literature, with data obtained from 109 sites where the event is unambiguously recorded (either through preservation of the ubiquitous NCIE, or where biostratigraphy and lithostratigraphic correlation unambiguously supports a T-OAE age) (Fig. 2). Strictly, the NCIE and T-OAE are not synonymous because evidence for deoxygenation is diachronous (Ruebsam and Schwark, 2024), or indeed absent at many sites (Kemp et al., 2022). In this study we use the NCIE to define the hyperthermal event ('Jenkyns Event' in the definition by Reolid et al., 2020) sensu stricto because the NCIE chronostratigraphically delineates the interval of global carbon cycle disturbance, and it is within the NCIE that evidence for seawater warming, $CO_2$ rise and hydroclimate change has been observed (Fig. 1; e.g., Bailey et al., 2003; McElwain et al., 2005; Izumi et al., 2018; Ruebsam et al., 2020a, 2020b).

The geographic distribution of available sites is biased (Fig. 2), with most studied sections occurring in Europe (75). The remaining 34 sites are unevenly distributed between North Africa (12), Asia (11), North and South America (7), Arctic (3), and Middle East (1). The depositional environment and dominant facies for each site are taken from the published sources, and are provided in Table S1. Most sites (80) are classified as shallow marine (i.e. nearshore to shelf environments, likely <200 m water depth) (Fig. 2), though water depth for many sites is uncertain. Twenty-three shallow water sites are carbonate-dominated platform/ramp environments, and 6 sites are non-marine (lacustrine) (Fig. 2).

We focus on potential hydroclimate changes associated with the NCIE in a broad sense, and accordingly group the evidence into 5 categories: 1) evidence for sedimentary event deposits that could be linked to storm activity (e.g., tempestite beds, hummocky(−swaley) cross-stratification), 2) evidence for sedimentary event deposits that could be linked to changes in the style or magnitude of sediment delivery to basins (i.e. hyperpycnites, mass flow deposits and turbidites), 3) evidence for changes in terrigenous fluxes that may relate to changes in fluvial sediment loads, 4) evidence for changes in hinterland chemical weathering, and 5) evidence for changes in seawater salinity that may relate to changes in freshwater runoff.

It is important to note that the above evidence categories are not unambiguously indicative of hydroclimate. The formation and preservation of storm deposits, for instance, is strongly dependent on depositional conditions (such as water depth) and sediment type. Similarly, mass flow deposits commonly have tectonic drivers, and fluvial sediment loads (and hinterland weathering/erosion) are also sensitive to tectonics. However, our aim in building the compilation is to present the available data that might be linked to hydroclimate, and then critically evaluate these data in our ensuing discussion (Section 4). The evidence we obtained is summarised in Table 1, with full details provided in the Supplementary Information (Table S1). The proxies available to determine potential changes in hydroclimate related to these evidence categories are varied (e.g., geochemical, sedimentological and paleontological), and in general the published evidence is objectively recorded based on the inferences drawn by the authors of the original studies, rather than re-interpreted here (though see Section 4 for a full discussion).

Evidence for potential hydroclimate change across the NCIE is classed as either absent, weak or strong, depending on: 1) data availability, 2) the reliability of the data as an indicator of hydroclimate, 3) whether or not an observed change in hydroclimate across the event is clearly resolved by the data, and 4) whether or not an observed change in hydroclimate was unambiguously contemporaneous with the NCIE. For the latter two considerations, we note that many studies provide high-resolution data within the NCIE but fewer data below and above, thus making it difficult to evaluate whether any actual change in hydroclimate was associated with the NCIE itself. The specific evidence for hydroclimate changes for each site is provided in Table S1. For some sites, there are no data available that provide hydroclimate information (full details in Table S1).

## 3. Results

Table 1 and Fig. 3 summarise the evidence for potential hydroclimate change through the NCIE for the 109 T-OAE sites. Full details of all the evidence is provided in Table S1, and in this section we provide a broad summary of this evidence. A majority of sites (71) have weak or strong evidence for hydroclimate change correspondent to at least one of the five defined evidence categories (Table 1, Fig. 3). The vast majority of these sites (69) contain evidence that can, potentially, be interpreted to reflect an increase in hydrological cycling, i.e. increased storm activity, event bed deposition, terrigenous fluxes, weathering and runoff under inferred wetter/more humid conditions (Fig. 3). Seven sites contain evidence consistent with a possible reduction in hydrological cycling (i.e. decreased storm activity, event bed deposition, terrigenous fluxes, weathering and runoff under inferred drier conditions). In all but 2 of these sites (Chaabet El Attaris in Tunisia and Skladaná Skala in Slovakia), the evidence for a decrease in hydrological cycling co-occurs with evidence from other hydroclimate indicators for an increase in hydrological cycling.

Thirty-seven sites show weak or strong evidence for an increase in storm deposits during the NCIE (Table 1, Fig. 3). This evidence is based on the occurrence of sedimentary deposits such as tempestites and/or hummocky cross-stratification (HCS) within the NCIE interval. Data on storm deposits are mapped on Fig. 4. Sites where evidence is considered strong (19) are distributed globally in both hemispheres (Fig. 4). These sites show a clear increase in storm-related deposits within the NCIE relative to the surrounding strata. For the other 18 sites, the evidence is weak because storm-related deposits are either rare (perhaps just 1 or 2 storm-related beds within the NCIE) or because it is unclear if storm deposits are significantly more abundant within the NCIE relative to the pre- and post-event strata. A single site (Valdorbia, Italy) shows strong evidence for a decrease in storm deposit abundance during the NCIE.

Nineteen sites show strong (15) or weak (4) evidence for increased deposition of turbidites/mass flow deposits (including hyperpycnites) within the NCIE. Data are mapped on Fig. 4. As with the data on storm deposits, the evidence is globally distributed, though largely restricted to deep water ocean margin sites (Fig. 4). For 8 sites, it is unclear if the sedimentary structures recorded were the product of storms or mass flow events (these are labelled with question marks on Table 1). A single site (Chaabet El Attaris) shows strong evidence for a decrease in turbidite deposits during the NCIE.

Twenty-two sites show weak (2) or strong (20) evidence for an increase in chemical weathering in the NCIE, as determined from inorganic geochemistry (e.g., increase in chemical index of alteration

**Table 1**
Summary table of evidence for potential hydroclimate changes at each of the 109 studied T-OAE sites. Evidence in capital letters = strong evidence, lowercase = weak evidence (see Section 2 for details). Blanks indicate no relevant data or no clear evidence for any change in hydroclimate. See Table S1 for full descriptions of hydroclimate data available from each site, as well as depositional environment interpretation. Sites are ordered by latitude and region (sites 1–86 = Europe/North Africa, sites 87–109 = rest of the world, see Fig. 2 for locations). See Fig. 3 for a bar chart of these data.

| Site number ( Fig. 2) | Site name | Region | Country | Key reference(s) | Evidence for change in storm deposit abundance | Evidence for change in turbidite/ mass flow abundance | Evidence for change in terrigenous flux | Evidence for change in weathering | Evidence for change in runoff inferred from paleosalinity |
|---|---|---|---|---|---|---|---|---|---|
| 1 | 34/10–35 | Europe | Norway | van de Schootbrugge et al. (2019) | | | | | |
| 2 | Bornholm | Europe | Denmark | Hesselbo et al. (2000) | | | | | |
| 3 | Brody-Lubiena | Europe | Poland | Hesselbo and Pieńkowski (2011); Brański (2010, 2012) | | | Increase | INCREASE | |
| 4 | Mechowo | Europe | Poland | Hesselbo and Pieńkowski (2011); Brański (2010, 2012) | | | Increase | INCREASE | |
| 5 | Gorzow Wielkpolski | Europe | Poland | Hesselbo and Pieńkowski (2011) | | | Increase | | |
| 6 | Suliszowice | Europe | Poland | Hesselbo and Pieńkowski (2011); Brański (2010, 2012) | | | Increase | INCREASE | |
| 7 | Parkoszowice | Europe | Poland | Hesselbo and Pieńkowski (2011); Pieńkowski et al. (2016) | | | Increase | | |
| 8 | Kozłowice | Europe | Poland | Leonowicz (2011); Hesselbo and Pieńkowski (2011) | Increase | | | | |
| 9 | Schandelah | Europe | Germany | van de Schootbrugge et al. (2018) | | | | | |
| 10 | F11–01 | Europe | Netherlands | Trabucho-Alexandre et al. (2012); Houben et al. (2021) | Increase | | | | |
| 11 | L05–04 | Europe | Netherlands | Trabucho-Alexandre et al. (2012) | Increase | | | | |
| 12 | Raasay | Europe | Scotland | Chen et al. (2021); Morton and Hudson (1995) | Increase | | INCREASE | INCREASE | |
| 13 | Zazriva | Europe | Slovakia | Suan et al. (2018) | ?Increase | ?Increase | | | |
| 14 | Yorkshire | Europe | England | Kemp et al. (2005); Ghadeer and Macquaker (2011, 2012); Wignall et al. (2005); Thibault et al. (2018); Remírez and Algeo (2020); Slater et al. (2019) | Increase | | | | INCREASE |
| 15 | Dove's Nest | Europe | England | Trabucho-Alexandre et al. (2023) | Increase | | | | |
| 16 | RWK-01 | Europe | Netherlands | Houben et al. (2021) | | | | | |
| 17 | Aubach | Europe | Germany | Hougård et al. (2021); Schieber et al. (2010) | Increase | | | | |
| 18 | Dotternhausen | Europe | Germany | Röhl et al. (2001); Mattioli et al. (2004, 2008); Schmid-Röhl et al. (2002) | ?INCREASE | ?INCREASE | | | INCREASE |
| 19 | Réka Valley | Europe | Hungary | Baranyi et al. (2016); Ruebsam et al. (2018); Raucsik and Varga (2008) | | Increase | INCREASE | INCREASE | Increase |
| 20 | FR-210-078 | Europe | Luxemburg | Ruebsam et al. (2014) | | | | | |
| 21 | Denkingen | Europe | Germany | Suan et al. (2015) | | | | | |
| 22 | Mochras Farm | Europe | Wales | Xu et al. (2018); Ullmann et al. (2021); van de Schootbrugge et al. (2005); Menini et al. (2021) | ?INCREASE | ?INCREASE | INCREASE | INCREASE | INCREASE |
| 23 | EST433 | Europe | France | Lézin et al. (2013) | | | | | Increase |
| 24 | Rietheim | Europe | Switzerland | Fantasia et al. (2018a); Fantasia et al. (2019a); Montero-Serrano et al. (2015) | ?INCREASE | ?INCREASE | INCREASE | INCREASE | |
| 25 | HTM-102 | Europe | France | van Breugel et al. (2006); Mattioli et al. (2008) | Increase | | | | INCREASE |
| 26 | Riniken | Europe | Switzerland | Fantasia et al. (2018a); Fantasia et al. (2019a) | ?INCREASE | ?INCREASE | INCREASE | INCREASE | INCREASE |
| 27 | Winterborne Kingston | Europe | England | Jenkyns et al. (2001); Jenkyns and Clayton (1997) | | | | | |
| 28 | 18/25-1 | Europe | Ireland | Silva et al. (2017) | | | | | |

(*continued on next page*)

**Table 1** (*continued*)

| Site number (Fig. 2) | Site name | Region | Country | Key reference(s) | Evidence for change in storm deposit abundance | Evidence for change in turbidite/ mass flow abundance | Evidence for change in terrigenous flux | Evidence for change in weathering | Evidence for change in runoff inferred from paleosalinity |
|---|---|---|---|---|---|---|---|---|---|
| 29 | Gipf | Europe | Switzerland | Fantasia et al. (2018a); Fantasia et al. (2019a) | ?INCREASE | ?INCREASE | INCREASE | INCREASE | |
| 30 | Skladaná Skala | Europe | Slovakia | Müller et al. (2020) | | | Decrease | | |
| 31 | Sancerre-Couy | Europe | France | Hermoso and Pellenard (2014); Hermoso et al. (2013); Clémence et al. (2015) | | | Increase | INCREASE | INCREASE |
| 32 | Lafarge | Europe | France | Suan et al. (2013); Dera et al. (2009); Martin et al. (2021) | INCREASE | | | INCREASE | |
| 33 | Creux De L'Ours | Europe | Switzerland | Fantasia et al. (2018a); Fantasia et al. (2019a) | ?INCREASE | ?INCREASE | INCREASE | INCREASE | INCREASE |
| 34 | Suèges | Europe | France | Fonseca et al. (2018) | | | | | |
| 35 | Saint Paul Des Fonts | Europe | France | Mailliot et al. (2009); Krencker et al. (2015); Bomou et al. (2021) | Increase | | | | Increase |
| 36 | Bächental | Europe | Austria | Neumeister et al. (2015); Suan et al. (2016) | | INCREASE | | | INCREASE |
| 37 | Caylus | Europe | France | Fonseca et al. (2018) | | | | | INCREASE |
| 38 | Cuers | Europe | France | Léonide et al. (2012) | | | | | |
| 39 | Tournadous | Europe | France | Mailliot et al. (2009); Krencker et al. (2015) | Increase | | | | INCREASE |
| 40 | West Rodiles | Europe | Spain | Fernández-Martínez et al. (2021); Rodrigues et al. (2020b) | ?Increase | ?Increase | INCREASE | | |
| 41 | Roqueredonde | Europe | France | Bomou et al. (2021) | | | INCREASE | INCREASE | Increase |
| 42 | La Almunia | Europe | Spain | Gahr (2005); Gómez et al. (2008) | Increase | | | | |
| 43 | Barranco de la Cañada | Europe | Spain | Gahr (2005); Piazza et al. (2020); Ullmann et al. (2020) | | | | | |
| 44 | Barranco de la Puta | Europe | Spain | Fürisch et al. (2001) | | | | | |
| 45 | Alcabideque | Europe | Portugal | Rodrigues et al. (2016) | | | INCREASE | Decrease | |
| 46 | Longarone | Europe | Italy | Bellanca et al. (1999) | | Increase | | | |
| 47 | Rabaçal | Europe | Portugal | Krencker et al. (2015); Rodrigues et al. (2020a) | INCREASE | | INCREASE | | |
| 48 | Dogna | Europe | Italy | Jenkyns et al. (2001) | | | | | |
| 49 | Breggia | Europe | Switzerland | Fantasia et al. (2018a); Fantasia et al. (2019a); Dera et al. (2009) | | | Increase | DECREASE | |
| 50 | Es Cosconar | Europe | Spain | Rosales et al. (2018) | | | | | |
| 51 | Peniche | Europe | Portugal | Hesselbo et al. (2007); Fantasia et al. (2019b); Rodrigues et al. (2020a); Correia et al. (2017); Mattioli et al. (2008); Suan et al. (2008); Wright and Wilson (1984); Font et al. (2022) | | INCREASE | INCREASE | INCREASE | INCREASE |
| 52 | Monte Mangart | Europe | Italy | Sabatino et al. (2009) | | | | | |
| 53 | Colma di Malcesine | Europe | Italy | Woodfine et al. (2008) | | | Increase | | |
| 54 | Sega d'Ala | Europe | Italy | Woodfine et al. (2008) | | | Increase | | |
| 55 | Madonna della Corona | Europe | Italy | Woodfine et al. (2008) | | | Increase | | |
| 56 | Gajum | Europe | Italy | Erba et al. (2022) | | | | | |
| 57 | Sogno | Europe | Italy | Erba et al. (2022); Gambacorta et al. (2023) | | | INCREASE | INCREASE | INCREASE |
| 58 | Kovk | Europe | Slovenia | Ettinger et al. (2021) | | | | | |
| 59 | Fuente La Vidriera | Europe | Spain | Rodrigues et al. (2019); Palomo Delgado et al. (1985); Dera et al. (2009); Rodríguez-Tovar and Uchman (2010) | | | Increase | | |
| 60 | Colle d'Orlando | Europe | Italy | Mattioli and Pittet (2004) | Increase | | | | |
| 61 | La Cerradura | Europe | Spain | Rodrigues et al. (2019); Reolid et al. (2019) | | | INCREASE | | |
| 62 | Velebit-A | Europe | Croatia | Sabatino et al. (2013) | | | | | |
| 63 | Valdorbia | Europe | Italy | Sabatino et al. (2009); Monaco et al. (1994); | DECREASE | INCREASE | INCREASE | | |

(*continued on next page*)

**Table 1** (*continued*)

| Site number (Fig. 2) | Site name | Region | Country | Key reference(s) | Evidence for change in storm deposit abundance | Evidence for change in turbidite/ mass flow abundance | Evidence for change in terrigenous flux | Evidence for change in weathering | Evidence for change in runoff inferred from paleosalinity |
|---|---|---|---|---|---|---|---|---|---|
| 64 | Pozzale | Europe | Italy | Monaco (2016); Dera et al. (2009); Monaco (1992) Mattioli and Pittet (2004); Mattioli et al. (2004); Dera et al. (2009); Morettini (1998) | Increase | | | | INCREASE |
| 65 | Velebit-B | Europe | Croatia | Sabatino et al. (2013) | | | | | |
| 66 | Fonte Cerro | Europe | Italy | Mattioli and Pittet (2004) | Increase | | | | |
| 67 | Gornje Jelenje | Europe | Croatia | Sabatino et al. (2013) | | | | | |
| 68 | Monte Sorgenza | Europe | Italy | Woodfine et al. (2008) | | | | | |
| 69 | Mercato San Severino | Europe | Italy | Trecalli et al. (2012) | | | | | |
| 70 | Chionistra | Europe | Greece | Kafousia et al. (2014) | | | | | |
| 71 | Petousi | Europe | Greece | Kafousia et al. (2014) | | | | | |
| 72 | Livartzi | Europe | Greece | Kafousia et al. (2011) | | | | | |
| 73 | Toka | Europe | Greece | Kafousia et al. (2014) | | | | | |
| 74 | Taguendouft | Africa | Morocco | Krencker et al. (2020) | INCREASE | | INCREASE | | |
| 75 | Kastelli | Europe | Greece | Kafousia et al. (2011) | | | | | |
| 76 | Tabant | Africa | Morocco | Krencker et al. (2022) | Increase | | | | |
| 77 | Chaabet El Attaris | Africa | Tunisia | Ruebsam et al. (2021); Reolid et al. (2021) | | DECREASE | Decrease | | |
| 78 | Amellago | Africa | Morocco | Bodin et al. (2010, 2011) | | | | | |
| 79 | Talghemt | Africa | Morocco | Boulila et al. (2019) | | INCREASE | | | |
| 80 | Ouguerd Zegzaoune | Africa | Morocco | Krencker et al. (2015) | INCREASE | | INCREASE | | |
| 81 | Tamtetoucht | Africa | Morocco | Krencker et al. (2020) | INCREASE | | INCREASE | | |
| 82 | Ratnek El Kahla | Africa | Algeria | Reolid et al. (2012) | | | Increase | | |
| 83 | Toksine | Africa | Morocco | Krencker et al. (2015) | INCREASE | | | | |
| 84 | Aghbalou N'Kerdous | Africa | Morocco | Krencker et al. (2020) | INCREASE | | INCREASE | | |
| 85 | Foum Tillicht | Africa | Morocco | Bodin et al. (2016) | | INCREASE | | | |
| 86 | Tahria N'Dades | Africa | Morocco | Krencker et al. (2022) | | | | | |
| 87 | Kelimyar River | Arctic | Russia | Suan et al. (2011); Nikitenko et al. (2013) | | | | | |
| 88 | Polovinnaya River | Arctic | Russia | Suan et al. (2011) | | | | | |
| 89 | Anabar Bay | Arctic | Russia | Suan et al. (2011) | | | | | |
| 90 | ZK01 | Asia | China | Liu et al. (2020b) | | | Increase | Increase | INCREASE |
| 91 | Anya | Asia | China | Jin et al. (2022b); Li et al. (2023); Baranyi et al. (2024) | | | INCREASE | INCREASE | |
| 92 | Sichuan Core B | Asia | China | Xu et al. (2017) | | | | | |
| 93 | LQ104X | Asia | China | Liu et al. (2022b); Liu et al. (2022a); Liu et al. (2020a) | INCREASE | INCREASE | INCREASE | INCREASE | Increase |
| 94 | Sichuan Core A | Asia | China | Xu et al. (2017); Xu et al. (2021) | | | | | Increase |
| 95 | Sakuraguchi-Dani | Asia | Japan | Izumi et al. (2018); Kemp et al. (2019); Kemp and Izumi (2014); Chen et al. (2023a) | INCREASE | INCREASE | INCREASE | INCREASE | |
| 96 | Dameigou | Asia | China | Lu et al. (2020) | | | | Increase | |
| 97 | 6–32-75-5 W6 | North America | Canada | Them et al. (2018); Asgar-Deen et al. (2003) | | | | | |
| 98 | Haida Gwaii | North America | Canada | Them et al. (2017b); Caruthers et al. (2011) | | | | | |
| 99 | 1–35-62-20 W5 | North America | Canada | Them et al. (2018); Asgar-Deen et al. (2003) | | | | | |
| 100 | Bighorn Creek | North America | Canada | Them et al. (2017b) | | | INCREASE | | |
| 101 | Bilong Co | Asia | China | Fu et al. (2014, 2016); Xia et al. (2021) | | | INCREASE | | INCREASE |
| 102 | Suobucha | Asia | China | Yi et al. (2023); Nie et al. (2023) | | | INCREASE | INCREASE | INCREASE |
| 103 | Sakahogi | Asia | Japan | Ikeda et al. (2018) | | | | | |
| 104 | Khashm adh Dhibi | Middle East | Saudi Arabia | Alnazghah et al. (2022); Al-Hussaini et al. (2021) | INCREASE | | INCREASE | INCREASE | |
| 105 | Nianduo | Asia | China | Han et al. (2018, 2022) | INCREASE | | INCREASE | | |
| 106 | Wölong | Asia | China | Han et al. (2018) | INCREASE | | | | |

(*continued on next page*)

**Table 1** (*continued*)

| Site number ( Fig. 2) | Site name | Region | Country | Key reference(s) | Evidence for change in storm deposit abundance | Evidence for change in turbidite/ mass flow abundance | Evidence for change in terrigenous flux | Evidence for change in weathering | Evidence for change in runoff inferred from paleosalinity |
|---|---|---|---|---|---|---|---|---|---|
| 107 | Asientos | South America | Chile | Fantasia et al. (2018b) | INCREASE | INCREASE | INCREASE | DECREASE | |
| 108 | El Peñon | South America | Chile | Fantasia et al. (2018b) | Increase | INCREASE | INCREASE | DECREASE | |
| 109 | Arroyo Lapa | South America | Argentina | Al-Suwaidi et al. (2010, 2016) | | | | | |

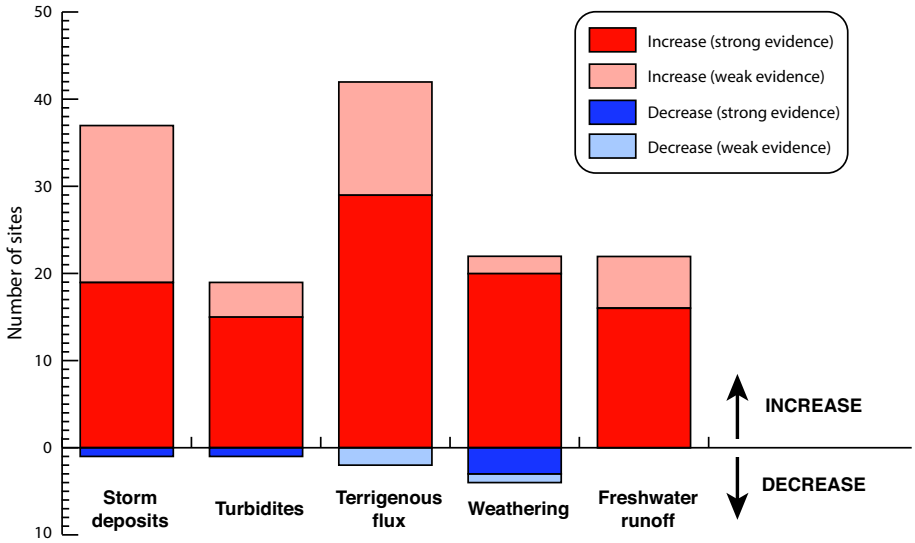


**Fig. 3.** Summary bar chart of evidence for potential hydroclimate changes from the studied T-OAE sites. The majority of sites yielding data on potential hydroclimate change preserve evidence consistent with an increase in hydrological cycling during the T-OAE NCIE (i.e., an increase in storm deposits, turbidites, terrigenous flux, weathering, or freshwater runoff). See Section 4 for a full discussion.

values) or clay mineral assemblages (i.e. an increase in relative abundance of kaolinite) (Table 1, Fig. 3). Data on weathering are mapped on Fig. 5, and there is no clear geographic pattern. Four sites (Breggia in Italy, Alcabideque in Portugal, and Asientos and El Peñon in Chile) show strong or weak evidence for a reduction in chemical weathering intensity during the NCIE.

Forty-two sites show weak (13) or strong (29) evidence for an increase in terrigenous flux coincident with the NCIE (Table 1, Fig. 3). Most commonly, the evidence for this is that palynological and/or petrographic data indicate a relative increase in the flux of terrestrial material during the NCIE (Table S1). Data on terrigenous fluxes are mapped on Fig. 6, and there is no clear geographic pattern. Two sites (Chaabet El Attaris and Skladaná Skala) show weak evidence for a decrease in terrigenous flux during the NCIE.

Twenty-two sites show weak (6) or strong (16) evidence for lowered surface water salinity and/or water column stratification during the NCIE, potentially related to increased freshwater runoff (Table 1, Fig. 3). Evidence for decreased salinity is most typically based on nannofossil assemblage changes (e.g., an increase in the abundance of freshwater-tolerant *Calyculus* coccolithophores) or geochemistry (B/Ga ratios, organic geochemistry). For some sites, the evidence for salinity decrease is more indirect, and based on the deduction that inferred water column stratification (e.g., as proxied by gammacerane index) was related to salinity stratification, or because an observed decrease in belemnite $\delta^{18}O$ is too large to be fully accounted for by temperature rise alone. Data on salinity are mapped on Fig. 7. Data are concentrated in Europe, with a few studies carried out in Chinese basins (Fig. 7).

## 4. Discussion

### 4.1. Evidence for intensified storm activity during the T-OAE NCIE

The occurrence of storm deposits within lower Toarcian strata has been known from sites in the Lusitanian Basin in Europe for many years, where they were linked to tectonically driven sea level fall and deposition above storm wave-base (e.g., Duarte and Soares, 2002; Duarte, 2007; Duarte et al., 2007; Pittet et al., 2014). Suan et al. (2013) recognised that lower Toarcian tempestites were widespread in Europe, and largely stratigraphically restricted to the NCIE (e.g., Fig. 8). These observations, coupled with the low (<30°N) paleolatitude of the sites they studied, led to Suan et al. (2013) proposing that tempestite deposition was linked to an intensification of tropical cyclone activity due to warming. The same conclusion was reached by Krencker et al. (2015) through their wide-ranging analysis of sites in Europe and North Africa. Most recently, Yan et al. (2023) modelled T-OAE tropical cyclone distribution and potential intensity using a coupled global climate model, based on the inferred doubling of atmospheric $CO_2$ across the event (perhaps from ~500 ppm to ~1000 ppm, e.g., McElwain et al., 2005; Ruebsam et al., 2020b; Fig. 1). Similar to models of the modern climate system, this work predicted an increase in the frequency of intense tropical cyclones linked to $CO_2$ and temperature rise, and the predicted spatial pattern of storm activity was found to match well with the geological evidence (Yan et al., 2023).

Evidence for an increase in tempestite deposition in the NCIE is clearly widespread, with strong evidence recorded in shallow marine sections in Tibet (Nianduo and Wölong, Han et al., 2018), Japan

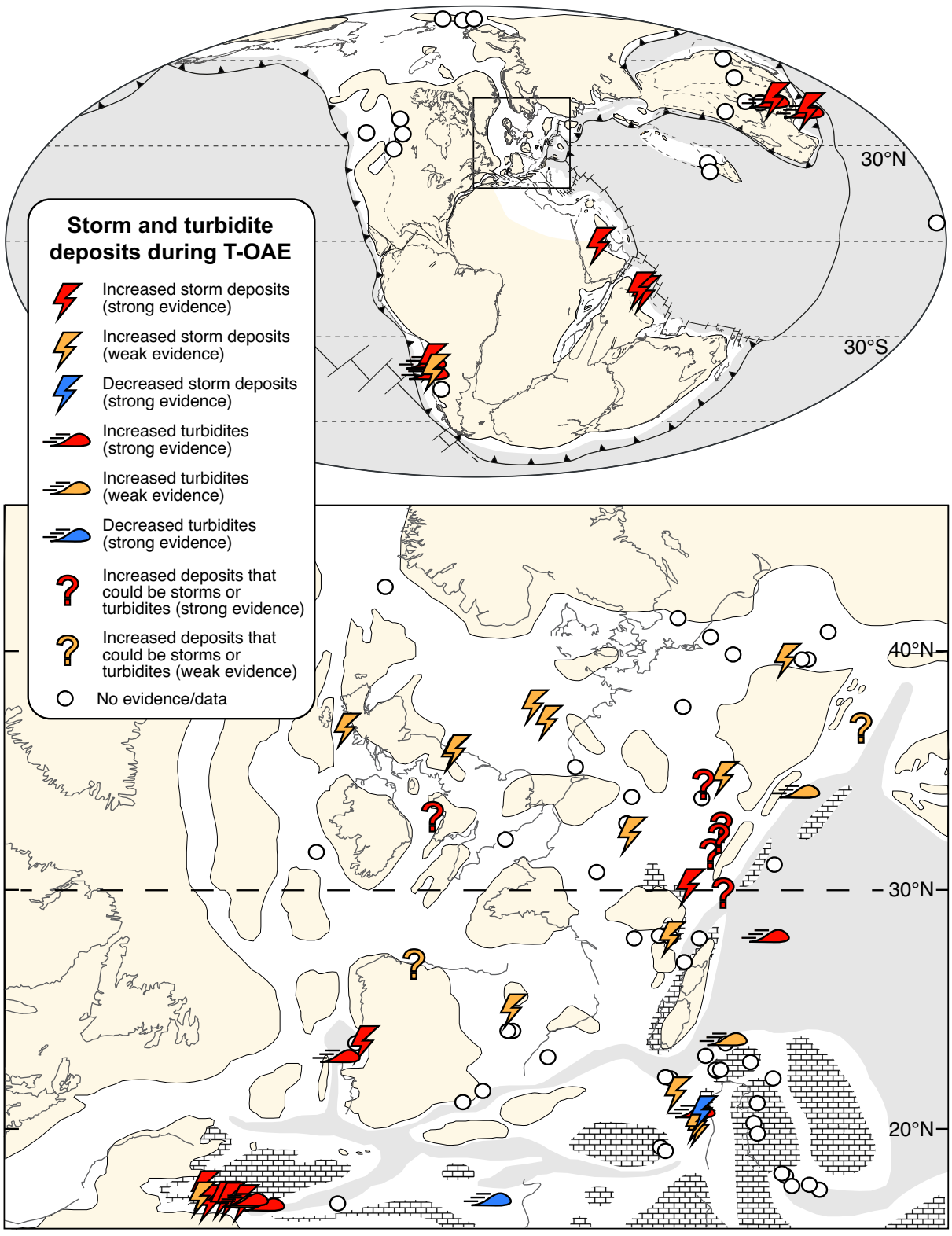


**Fig. 4.** Maps showing location of storm deposits, turbidites and other mass flow deposits during the T-OAE NCIE. Symbol colours reflect whether deposits increased or decreased in abundance relative to pre/post NCIE interval, and whether the evidence for these changes is weak or strong (see Section 2 for details). Question marks denote sites with deposits that may have formed during storms but could also be attributable to advective transport caused by turbidity currents/gravity flows (see Section 4.1 and Table 1). West Rodiles in northern Spain (site 40) contains deposits that may be tempestites or hyperpycnites (Fernández-Martínez et al., 2021). Data are summarised in Table 1, with full details in Table S1.

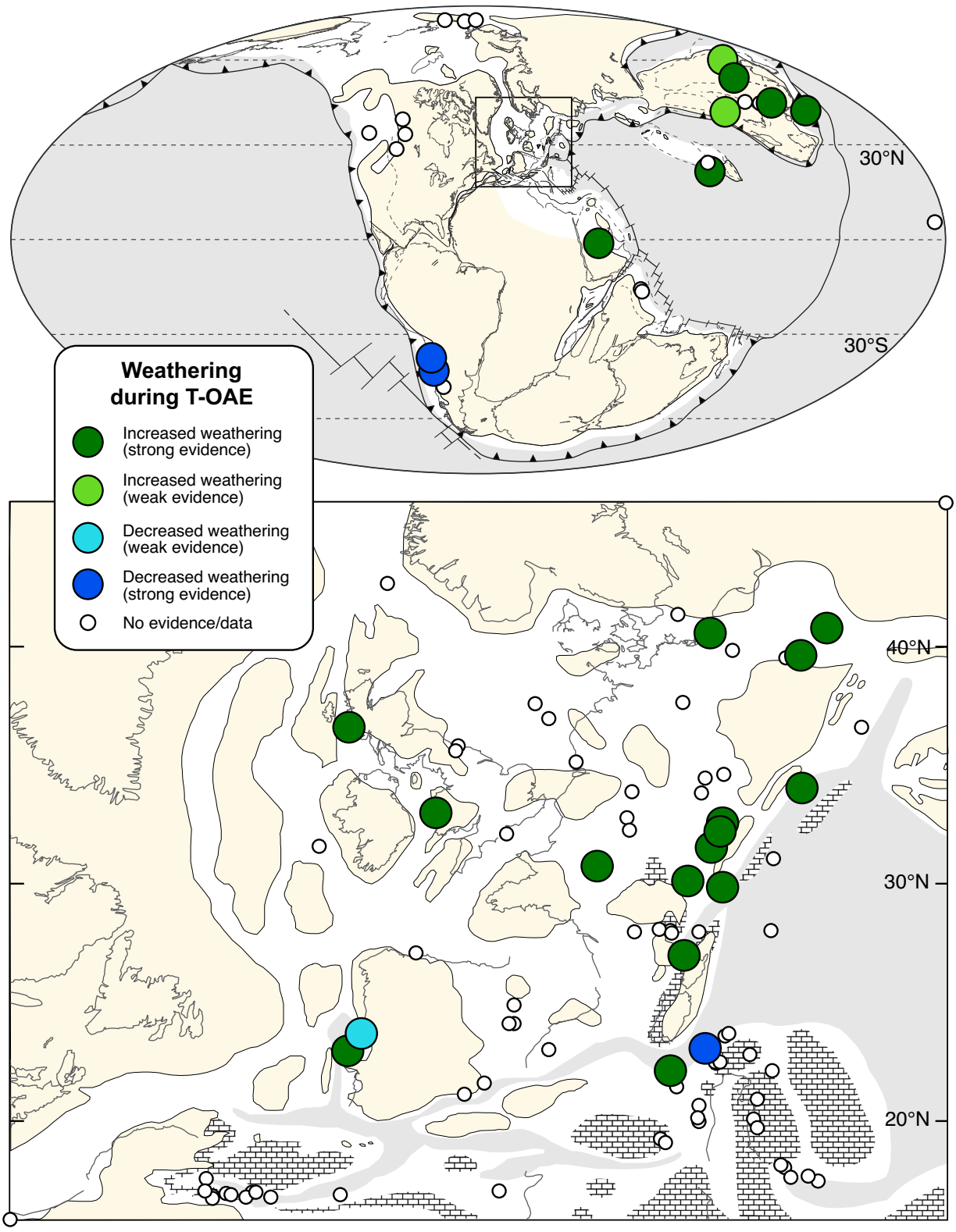


**Fig. 5.** Maps showing location of sites where evidence for a change in weathering is recorded across the T-OAE NCIE. Symbol colours reflect whether weathering increased or decreased during the NCIE relative to the pre/post NCIE interval, and whether the evidence for these changes is weak or strong (see Section 2 for details). Data are summarised in Table 1, with full details in Table S1.

(Sakuraguchi-dani, Izumi et al., 2018), Saudi Arabia (Khashm adh Dhibi, Al-Hussaini et al., 2021), and Chile (El Peñon and Asientos, Fantasia et al., 2018b) (Table 1, Figs. 4 and 8). A lacustrine site in the Sichuan Basin (LQ104X) also shows strong evidence for an increase in tempestite abundance during the NCIE (Liu et al., 2022b, see also Cui et al., 2023; Table 1, Fig. 4). Weak or strong evidence for increased storm deposits in the NCIE is recorded in over a quarter of all sites (29 out of the 109 studied), with 22 of these sites from Europe and the northwest Tethys region. At a further 8 sites, small-scale sedimentary structures (such as graded laminae with erosive bases) occur that may have formed during

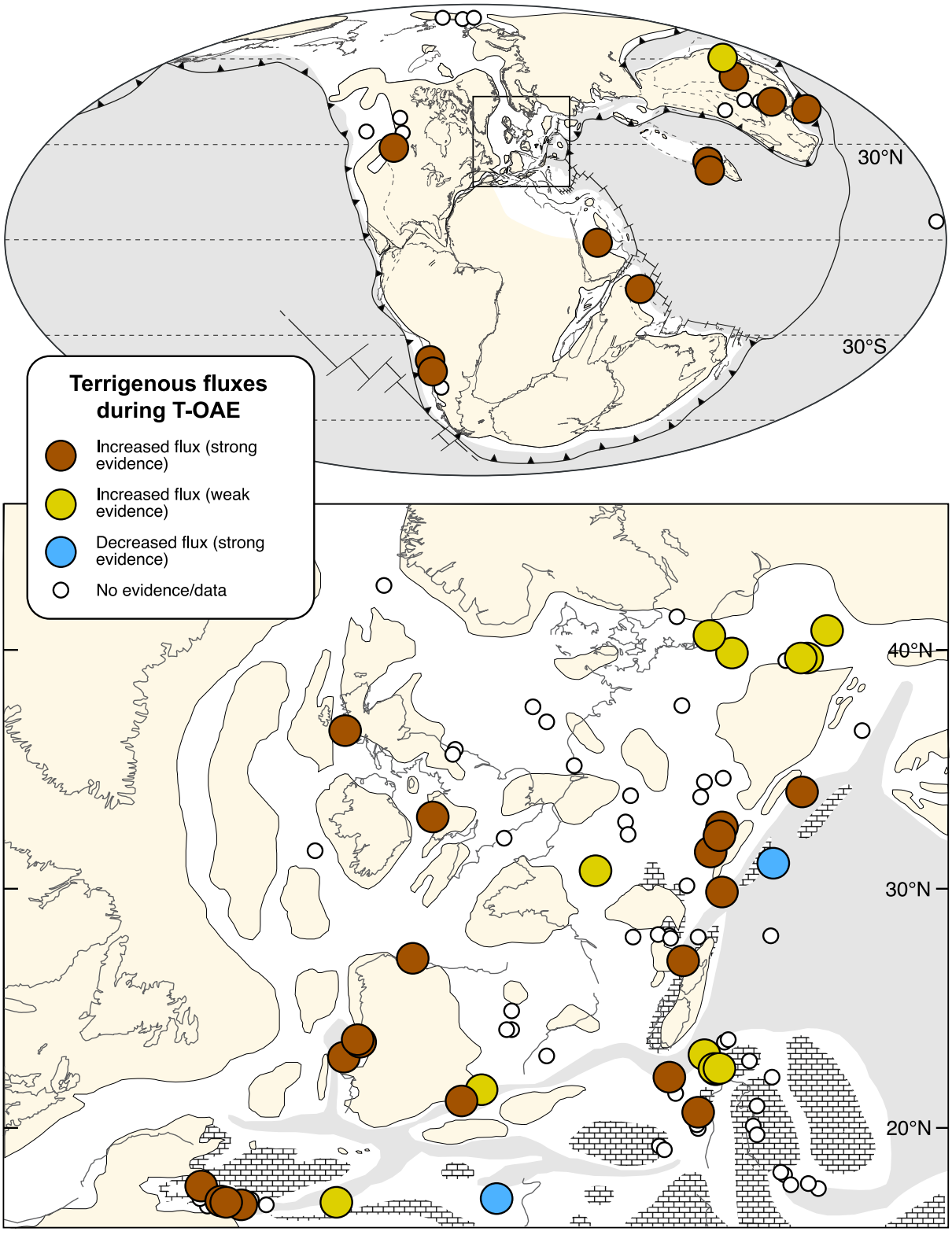


**Fig. 6.** Maps showing location of sites where evidence for a change in terrigenous fluxes is recorded across the T-OAE NCIE. Symbol colours reflect whether terrigenous fluxes increased or decreased during the NCIE relative to the pre/post NCIE interval, and whether the evidence for these changes is weak or strong (see Section 2 for details). Data are summarised in Table 1, with full details in Table S1.

storms but could also be attributable to advective transport caused by turbidity currents/gravity flows (e.g., Creux De L'Ours and Gipf in Switzerland in Fantasia et al., 2019a; Zazriva in Slovakia in Suan et al., 2018; Dotternhausen in Germany in Röhl et al., 2001; Fig. 2). Such flows could, of course, have been triggered by storms in any case – an issue discussed further in Section 4.2. Sections containing deposits with ambiguous genesis are labelled in Table 1 and on Fig. 4. Although the precise origin of many small-scale sedimentary structures can be ambiguous, at Yorkshire (UK) and Sakuraguchi-dani (Japan) detailed thin section work has enabled recognition of wave-enhanced sediment

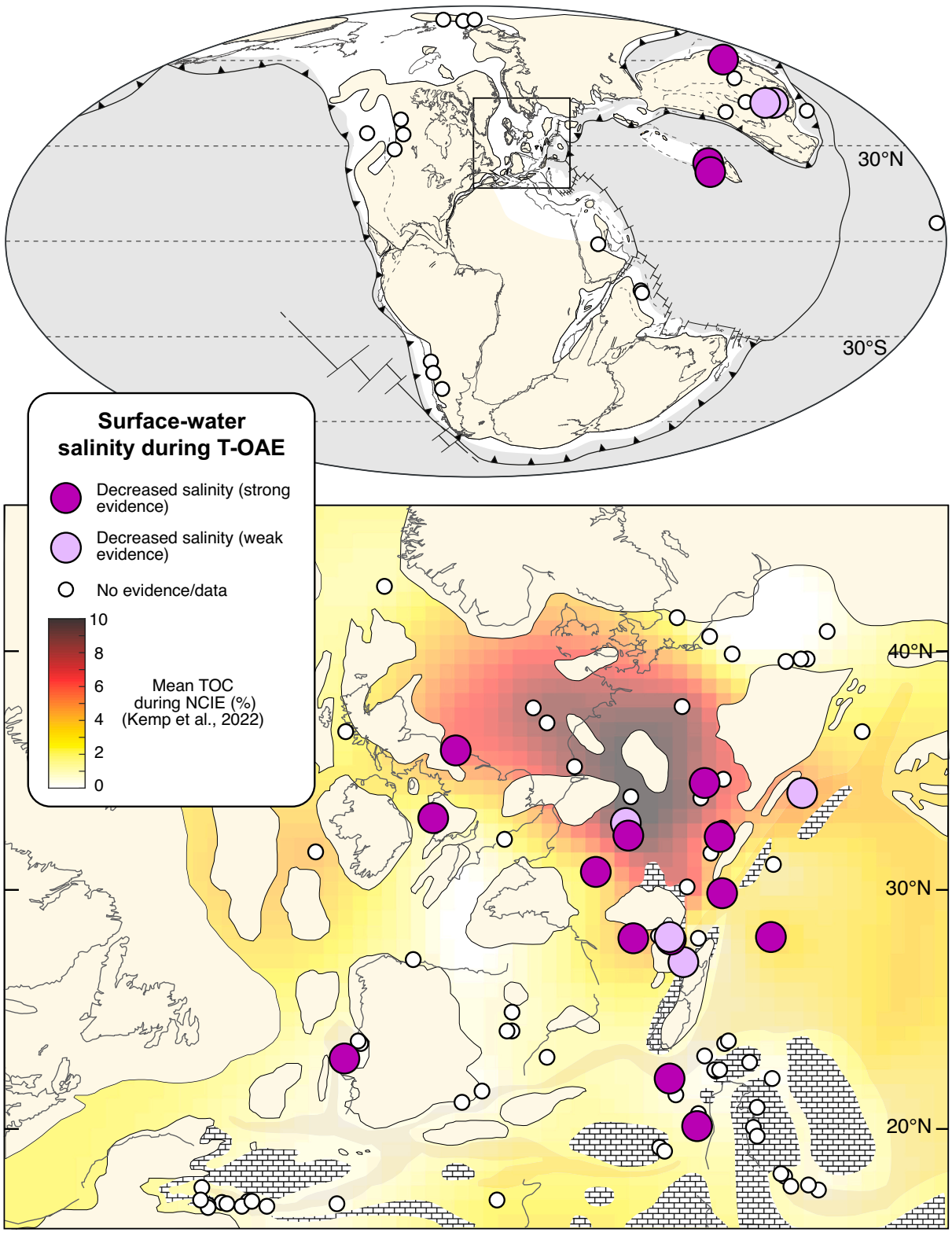


**Fig. 7.** Maps showing location of sites where evidence for a reduction in surface water salinity is recorded across the T-OAE NCIE. Symbol colours reflect whether the evidence is weak or strong (see Section 2 for details). The data on the Europe/North Africa inset map are plotted over a map of total organic carbon content (TOC) (from Kemp et al., 2022) to show the relationship between salinity and organic enrichment. Data are summarised in Table 1, with full details in Table S1.

gravity flows during the NCIE (Ghadeer and Macquaker, 2011; Izumi et al., 2018), indicating a link to storm activity (e.g., Fig. 8).

All but 4 sites that show strong evidence for an increase in storm activity in the NCIE were deposited at or below a paleolatitude of 30° (Fig. 4), consistent with previous deductions that these deposits were the product of tropical cyclones (Suan et al., 2013; Krencker et al., 2015; Han et al., 2018). Tropical cyclone genesis potential and intensity are proportional to the sea surface temperature over which they form (Gray, 1968; Emanuel, 2008), and the relatively high $CO_2$ and warm climate of the Toarcian (e.g., Ruebsam et al., 2020a; Ullmann et al., 2020; Nordt

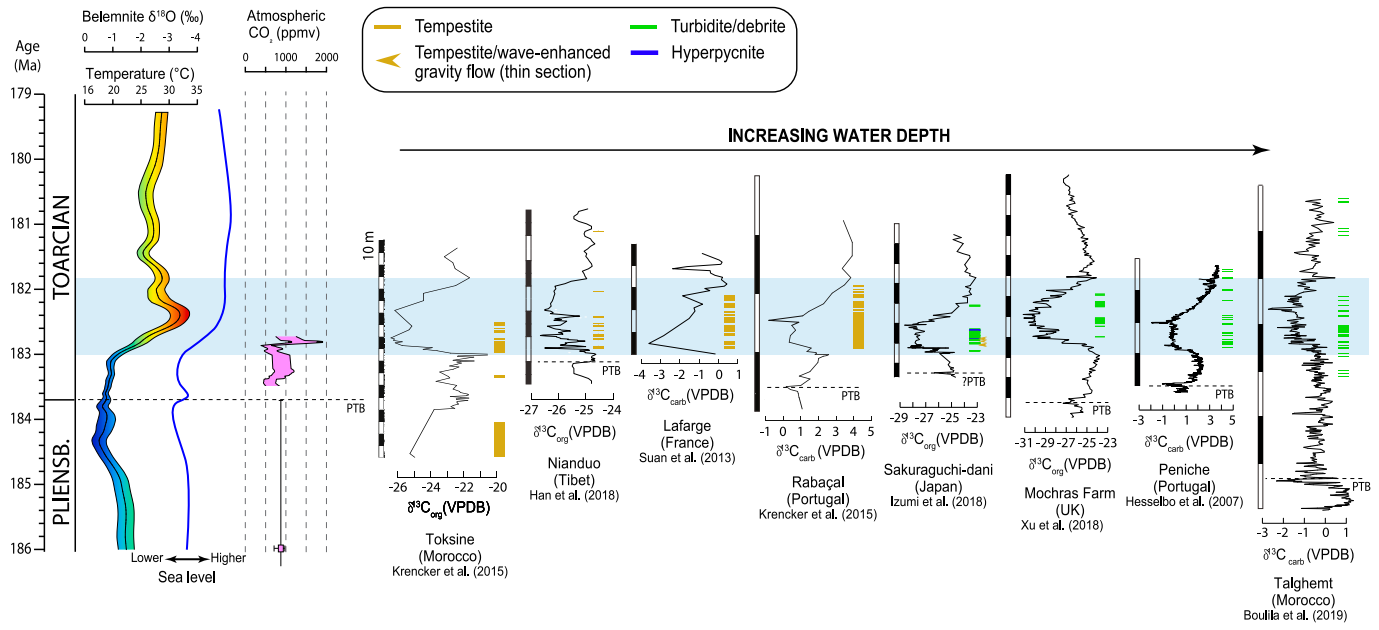


**Fig. 8.** T-OAE paleoclimate changes and data from sites showing evidence for increased storm deposits (tempestites) and other event deposits during the T-OAE NCIE. Belemnite oxygen isotope ($\delta^{18}O$) data and inferred paleotemperatures are from Ruebsam et al. (2019), with data smoothed using a 10 % LOESS function and with 2σ confidence interval based on bootstrapping (using same data as in Fig. 1). Atmospheric $pCO_2$ are from McElwain et al. (2005) and Steinthorsdottir and Vajda (2015) (as in Fig. 1). (Sea level curve is from Ruebsam et al. (2019). Sedimentology data for each site (i.e. stratigraphic position of tempestites, turbidites, hyperpycnites etc.) are plotted against organic (org) or carbonate (carb) carbon isotope ($\delta^{13}C$) data for each site. Position of the NCIE is shown with blue shading. Note the general restriction of tempestites, turbidites etc. to the NCIE in each section. Note also the general trend for tempestites to be more common in the relatively shallow water sections, and turbidites to be more common in the deeper water sections. See Section 4.2 for full discussion. PTB = Pliensbachian–Toarcian boundary. Figure modified from Yan et al. (2023). (For interpretation of the references to colour in this figure legend, the reader is referred to the web version of this article.)

et al., 2022) means that tropical cyclones would have readily formed both before and after the T-OAE (Yan et al., 2023). As such, the fact that tempestites are restricted to (or at least more commonly observed) within the NCIE strongly suggests an intensification of storms of sufficient magnitude to impinge on the sea floor and create a tempestite, and not simply an increase in storm frequency. This is consistent with modern empirical observations and climate models, which indicate that a warming climate causes an increase in the frequency of intense storms, and perhaps a decrease in the overall number of storms of any size (e.g., Knutson et al., 2020).

In our compilation, we find strong evidence for increased storm activity at sites that were likely situated at higher latitudes than modern day tropical cyclones typically occur (i.e. >30°, LQ104X, Sakuraguchi-dani, El Peñon and Asientos; Table 1, Fig. 4). Eight sites in Northern Europe with weak evidence for increased storm activity were deposited at paleolatitudes between 30 and 40°N (Fig. 4). Climate models have shown that higher atmospheric $CO_2$ would allow tropical cyclones to form and track at higher latitudes owing to higher sea surface temperatures and humidity, poleward jet stream shifts and expansion of Hadley circulation (Korty et al., 2017; Studholme et al., 2021). Models of tropical cyclone activity across the PETM predict a clear shift in tropical cyclone genesis to mid-latitude regions (i.e. 30–60°N) under elevated atmospheric $CO_2$ (Kiehl et al., 2021; Studholme et al., 2021). In fact, these models suggest that elevated $CO_2$ levels may have been detrimental to the generation of low-latitude tropical cyclones (Kiehl et al., 2021). This is because the $CO_2$ increase in low latitudes raises the temperature at the top of the atmosphere, consequently augmenting wind shear, which is unfavourable for tropical cyclone formation (Kiehl et al., 2021). Such a wholesale geographic shift in cyclone activity is not supported by existing T-OAE storm modelling (Yan et al., 2023), though further modelling of storm track behaviour during the T-OAE is needed. In detail, it is unclear if the mid-latitude storm deposits recognised in the compilation were the product of true tropical cyclones (i.e. formed as a result of rising warm and moist air over warm seas), or whether they reflect extratropical cyclones (synoptic-scale low-pressure systems) that form as a consequence of energy release at the boundary between air masses of contrasting temperature at mid-latitudes. Extratropical cyclones may respond to warming in a similar way to tropical cyclones; with warmer temperatures driving an increase in intensity (specifically precipitation intensity), and a poleward shift in storm tracks (e.g., IPCC, 2023). One site (Khashm adh Dhibi in Saudi Arabia) that has strong evidence of increased T-OAE storm deposits was situated at an inferred equatorial (~0°) latitude. Either the inferred paleolatitude of this site is incorrect or these deposits did not form from tropical cyclone activity, because tropical cyclones do not form at equatorial latitudes (<5°) owing to the lack of sufficient Coriolis force to allow cyclonic vortices to form (e.g., Studholme et al., 2021).

As noted above, early work that recognised tempestites in lower Toarcian strata in Portugal attributed their occurrence to sea level lowering, which could have allowed the basin floor (sediment surface) to be above storm wave-base (e.g., Duarte and Soares, 2002; Duarte, 2007; Duarte et al., 2007). However, sea level fall is unlikely to have been the cause of the NCIE storm deposits we observe globally because independent sequence stratigraphic and sedimentological work demonstrates a marked and protracted rise in global sea level through the NCIE (e.g. Hallam, 2001; Hesselbo, 2008; Thibault et al., 2018; Figs. 1 and 8). Moreover, evidence for increased abundance of tempestites is recorded in the lacustrine LQ104X site in the Sichuan Basin, China (Liu et al., 2022b). Sea level rise was coeval with warming (Figs. 1 and 8) and likely driven by thermosteric effects and/or the melting of high latitude ice sheets (e.g., Ruebsam et al., 2019; Nordt et al., 2022).

A single section (Valdorbia, Italy) shows evidence for a reduction in storm deposits across the NCIE (Table 1, Fig. 4). Here, HCS has been recorded in the middle Toarcian, but not in the underlying and deeper water argillaceous facies that record the NCIE (Monaco et al., 1994, see also Sabatino et al., 2009). Sea level rise may have prevented storms from impinging on the sea floor at this site during the NCIE, but the occurrence of turbidites in the NCIE instead invites speculation that

these were related to storm activity (Suan et al., 2013) – a possibility discussed further in Section 4.2.

One possible caveat to the inference that storm intensity was enhanced during the NCIE is that sea level rise could actually have increased the preservation potential of storm deposits. Notably, storm deposits formed in relatively shallow water well above fair weather wave-base may not be readily preserved owing to frequent sediment reworking by non-storm-related waves and tides. By contrast, sea level rise, and a consequent shift in deposition to below the depth at which ordinary waves and tides can typically influence the sediment surface, could have helped ensure the preservation of any storm events. In theory, then, the sea level rise at the T-OAE could have promoted storm deposit preservation. However, the abundance of evidence for increased storm activity from multiple sites and varying depositional environments supports the inference of a genuine change in weather at the T-OAE. In addition, sea level remained relatively high well after the NCIE (Figs. 1 and 8), but storm deposits are rare in the post-NCIE interval (e.g., Fig. 8). Sea level rise in the NCIE may have contributed to an increase in storm activity because the accompanying increase in the surface area of shallow epicontinental seas, coupled with extreme warming, would mean an increase in the size of areas conducive to evaporation and tropical cyclone development (PSUCLIM, 1999; Suan et al., 2013).

Enhanced sediment fluxes during warming (Section 4.3) can promote shelf instability via sediment loading of delta tops and shelves (e.g., Bailey et al., 2021), thus increasing the likelihood of sediment movement and tempestite generation during storm processes. Many recorded tempestites, particularly those in Portugal and Morocco, are in carbonate successions, and Suan et al. (2013) noted that carbonate platforms may have adopted homoclinal ramp geometries during the NCIE owing to low carbonate production. This in turn could favour efficient transport of material downslope (Suan et al., 2013). Indeed, the T-OAE carbonate crisis (especially the loss of reefs, Leinfelder et al., 2002) could have facilitated potentially wide redistribution of sediment during storms, further favouring tempestite preservation (e.g., Han et al., 2018).

### 4.2. *Turbidite deposition during the T-OAE and potential links to hydroclimate*

Turbidites and mass flow deposits can have both climatic and non-climatic origins, and distinguishing triggering mechanisms, especially in deep time, is difficult (e.g., Osleger et al., 2009). Nevertheless, there are both modern and geological examples of turbidites driven by major hydrologic events, including storms and intensified runoff (e.g., Osleger et al., 2009; Porcile et al., 2020; Jiang et al., 2022; Chen et al., 2023b). In our compilation, there is strong evidence that turbidites increased in abundance during the NCIE at 9 sites, with weak evidence for an increase at a further 2 sites (Table 1, Figs. 3 and 4). As noted in Section 4.1, 8 other sites show evidence for an increase in the occurrence of sedimentary structures during the NCIE that could have formed as a consequence of either storm activity or turbidite deposition (Fig. 4). Although the evidence for increased turbidite deposition in the NCIE is relatively rare (a maximum of 19 out of 109 sites), only a single site (Chaabet El Attaris in Tunisia) shows evidence for a decrease in turbidite abundance (Ruebsam et al., 2021) (Fig. 4).

Our compiled data suggests that storm activity during the NCIE may have directly triggered turbidity current events. Detailed sedimentological analysis across a basin transect from the High Atlas Basin of Morocco revealed that lower Toarcian storm deposits common in shallow water platform sections grade into turbidites in deeper outer platform and basinal sections, supporting a genetic link (Krencker et al., 2020; Fig. 8). In our compilation, this link is further supported by the observation that most (6 out of 7) shallow water sections in Morocco contain evidence for an increase in storm activity, and most (2 out 3) deep water sections from Morocco contain evidence for an increase in turbidite abundance (Table 1). Evidence for increased turbidite deposition coeval with the NCIE is particularly well-expressed at Talghemt (Figs. 4 and 8; Boulila et al., 2019), which was likely the deepest High Atlas Basin section in our compilation (Bodin et al., 2011; Krencker et al., 2020; Fig. 8). In the Lusitanian Basin of Portugal, gravity flow deposits occur in the NCIE interval in the hemipelagic Peniche section (Hesselbo et al., 2007; Fantasia et al., 2019b; Fig. 8), whereas HCS is absent (Wright and Wilson, 1984). By contrast, in shallower water Lusitanian Basin sections storm deposits are common in the NCIE (as noted in Section 4.1). Hesselbo et al. (2007) and Fantasia et al. (2019b) suggested that increased sediment supply and/or storms were a plausible driving mechanism of downslope mass sediment transport at Peniche. A similar genetic link between storm activity and turbidites has been proposed for the Valdorbia section in the Umbria-Marche Basin of Italy (Suan et al., 2013). As noted in Section 4.1, this is the only site to record a decrease in storm activity during the NCIE (Fig. 4). At this site, beds with HCS occur above (and possibly below) the NCIE, whereas the NCIE interval is instead characterised by deeper water facies containing abundant turbidites (Monaco, 1992; Monaco et al., 1994; Monaco, 2016). Deepening at this site may have led to sediment deposition well below storm wave-base, and it seems reasonable to infer that storm activity did not actually decrease during the NCIE, but that the basin deepening led instead to the deposition of turbidites that were triggered by storms affecting shallower waters (Suan et al., 2013). Taken together, the data support a genetic link between storm activity and turbidite deposition during the NCIE (Fig. 8).

Recent work by Bailey et al. (2021) has emphasized how turbidity currents can be triggered by increased sediment loading of shelves and slopes, without the need for extraneous physical triggering mechanisms such as storms (or indeed earthquakes or sea level falls). A putative link between warming, sediment supply increase and increased turbidite deposition has been established recently for the PETM in the North Sea Basin by Jin et al. (2022b). From the available data, it is not possible to establish whether turbidites at the T-OAE were triggered by enhanced sediment supply, or whether storms were the primary driving mechanism. Interestingly, Clare et al. (2015) found evidence that turbidites may have decreased in abundance during the PETM at a majority of sites (the findings of Jin et al. (2022b) notwithstanding). This decrease could be related, at least at some sites, to a switch from humid conditions to hotter and more arid conditions characterised by a reduction in fluvial runoff and sediment supply (Clare et al., 2015). By contrast, evidence for increased aridity during the T-OAE in our compilation is scarce, as discussed in Section 4.3.

Hyperpycnites are event deposits that result when a river in flood directly discharges a relatively dense mixture of fresh water and sediment into a water body. These hyperpycnal flow events can be triggered by storms. In the compilation, hyperpycnites are recorded within the NCIE in Sakuraguchi-dani in Japan (Izumi et al., 2018; Fig. 7), the lacustrine LQ104X site in China, and possibly at West Rodiles in Spain (Fernández-Martínez et al., 2021). Hyperpycnal flows are an important but underappreciated mechanism for transferring terrigenous sediment to marine and lacustrine basins. However, they can be difficult to unambiguously distinguish from purely gravity-driven flows and other deposits in the sedimentary record, and this means they may be commonly misinterpreted (Zavala and Pan, 2018). Given the evidence for both increased turbidite deposition and terrigenous fluxes during the NCIE (Figs. 4 and 6, Section 4.3), further work is needed to establish the prevalence and importance of hyperpycnites during the T-OAE.

Overall, our compilation supports a genetic link between hydroclimate change and turbidity current generation at the T-OAE, and that the restriction of abundant turbidites to the NCIE interval in some sites (typically deep water, Fig. 8) means their occurrence was likely caused by storm activity and/or perhaps enhanced sediment supply.

### 4.3. Hydrological cycling during the T-OAE NCIE inferred from weathering and terrigenous flux changes

A global increase in silicate chemical weathering at the T-OAE is readily predictable based on the relationship between rates of chemical weathering and temperature, which underpins the role of weathering as a chief feedback mechanism that regulates $CO_2$ and the Earth's temperature (Walker et al., 1981). Cohen et al. (2004) first presented evidence for a significant increase in rates of chemical weathering across the NCIE using Os-isotope analysis of mudrocks from the Yorkshire (UK) section. Although challenged by later work highlighting issues with the application of Os-isotopes in the restricted basinal setting of the Yorkshire section (e.g., McArthur et al., 2008), subsequent Os- and Ca-isotope data from globally distributed sections emphasizes a marked global increase in chemical weathering (e.g., Brazier et al., 2015; Percival et al., 2016; Them et al., 2017a; Kemp et al., 2020b; Fig. 1).

Data on local chemical weathering trends across the NCIE are relatively scarce. In the compilation, most sites where local chemical weathering has been evaluated show evidence for an increase (22 sites), and only 4 sites show a decrease (Breggia in Italy, Alcabideque in Portugal, and Asientos and El Peñon in Chile) (Fig. 5). There is no clear geographic pattern in the data (Fig. 5). Common evidence for increased chemical weathering includes an increase in the relative abundance of kaolinite versus illite, supporting earlier work by Dera et al. (2009) that highlighted increased kaolinite abundance during the early Toarcian at sites in Europe. Other studies have used element proxies for weathering, based primarily on the relative immobility of Al during chemical weathering relative to K, Ca, Na and Mg (e.g., chemical index of alteration) (Reolid et al., 2012; Fantasia et al., 2018a; Bomou et al., 2021; Liu et al., 2022b; Chen et al., 2023a).

An inferred increase in hydrolysing conditions necessary to explain a general increase in T-OAE chemical weathering is supported by modelling, which has suggested a 9 cm $yr^{-1}$ increase in mean global precipitation during the T-OAE in response to a doubling of $CO_2$ using a fully coupled ocean-atmosphere model (FOAM) (Dera and Donnadieu, 2012). Warming increases the moisture-holding capacity of the atmosphere, as dictated by the Clausius-Clapeyron equation (around 7 % increase for every 1 °C rise in temperature). As such, global atmospheric moisture could have increased by ~40 % during the ~5 °C warming potentially associated with the T-OAE. However, this does not translate to a ~ 40 % increase in mean precipitation (e.g., Trenberth et al., 2003; Myhre et al., 2019). Rather, warming increases the frequency and intensity of extreme precipitation (e.g., Myhre et al., 2019). Warming also increases the spatial heterogeneity of precipitation patterns, with wet areas becoming wetter and dry areas becoming drier (e.g., Roddell and Li, 2023). Continental interiors and other regions that are already sensitive to drought are thus likely to become more arid with increasing temperatures (IPCC, 2023). Aridification of certain regions during the T-OAE was predicted by the FOAM climate model used by Dera and Donnadieu (2012), and temperature increases in continental interiors may have been more extreme relative to seas owing to decreased soil moisture and a lack of convective precipitation (e.g., Peyser and Poulsen, 2008). Nevertheless, Dera and Donnadieu (2012) noted, as do we, a paucity of geological evidence for enhanced aridity across the T-OAE. This may be largely due to the fact that continental interior regions (and terrestrial sections generally) are rare in our compilation.

Some information on terrestrial hydrological changes across the T-OAE is available from palynology. Notably, it is well-known that in many places there was a proliferation of thermophilic and drought adapted flora in the Toarcian, especially *Cheirolepidiaceae* conifers producing *Classopollis* (Vakhrameyev, 1991; Zakharov et al., 2006; Slater et al., 2019; Deng et al., 2012, 2024; see also Ruebsam et al., 2019). Clear evidence of a *Classopollis* acme within the NCIE is observed at sites such as Yorkshire (UK), Anya (China), Sichuan Core A (China) and RWK-01 (Netherlands) (see Table S1). However, Slater et al. (2019) interpreted the NCIE *Classopollis* acme as indicative of enhanced seasonality, during which only drought-adapted taxa could proliferate, and not necessarily aridification. At the terrestrial Anya section in China, for instance, the *Classopollis* acme in the NCIE co-occurs with geochemical evidence for increased chemical weathering, and is thus consistent with an increase in wet and dry seasonal extremes (Li et al., 2023; Baranyi et al., 2024; Fig. 5). Deforestation during the NCIE (Baranyi et al., 2024) and the consequent more open landscape, coupled with seasonal precipitation extremes (flash floods), may further help explain the wash-in of inland thermophilic taxa like *Classopollis* to marine/lacustrine basins (Baranyi et al., 2024).

The magnitude of the global increase in chemical weathering rates across the NCIE has been estimated as 200–500 % (Brazier et al., 2015; Them et al., 2017a; Kemp et al., 2020b). However, it is important to note that such numbers do not reflect chemical weathering change per se, but the increased flux of radiogenic Os (of continental origin) necessary to drive the observed changes in the Os-isotope composition of global seawater (Kemp et al., 2020b). This distinction is important because if treated as a chemical weathering magnitude change, these numbers are far in excess of the weathering response reasonably expected for the probable changes in temperature and $CO_2$ that occurred during the T-OAE (see, for example, Penman et al., 2020 and references therein). As such, enhanced chemical weathering during the NCIE likely occurred in concert with significantly enhanced runoff fluxes, facilitating the large-scale movement of cations to the ocean. Dera and Donnadieu (2012) predicted a global annual surface water runoff increase of 3.5 cm $yr^{-1}$ under a doubling of $CO_2$. Enhanced physical weathering and runoff could be reasonably expected to also lead to enhanced fluvial sediment loads and thus increased sediment fluxes to marine basins, and indeed evidence for increased terrigenous sediment fluxes during the NCIE is the most common potential hydroclimate indicator in the compilation (Fig. 3). There is strong or weak evidence for increased terrigenous fluxes at 42 sites (Table 1, Fig. 6), and weak evidence for reduced terrigenous fluxes at just 2 sites (Chaabet El Attaris in Tunisia, Ruebsam et al., 2021, and Skladaná Skala in Slovakia, Müller et al., 2020).

Increased fluvial sediment loading and delivery to marine basins is a predicted consequence of warming (e.g., Syvitski et al., 2022), but the mechanisms are varied, complex, and latitude-dependent. In polar regions, increased fluvial sediment yields during warming are potentially extreme, and largely a consequence of ice-sheet and permafrost melting and thus liberation of previously immobile sediment (Syvitski and Milliman, 2007; Syvitski et al., 2022). However, in warmer lower latitude environments (i.e. like most of the sites in our compilation) a more complex interplay of precipitation, physical and chemical weathering, soil formation/loss and vegetation change dictates river sediment loads (Syvitski and Milliman, 2007; Syvitski et al., 2022). The evidence for increased terrigenous fluxes across the NCIE strongly suggest a link to climate, but the data do not necessarily imply wetter conditions (Syvitski and Milliman, 2007). Arid regions (where erosion can be high but weathering low) support rivers with extremely high sediment yields, for instance (e.g., Chapman and Finnegan, 2024). Moreover, even if the T-OAE terrigenous flux data do indeed reflect a signal of globally enhanced hydrological cycling under warmer and wetter conditions (as seems probable), the dataset may be biased. This is because the sedimentary record itself may preferentially record and preserve wetter conditions such as extreme flood events, and such conditions are likely to be associated with high terrigenous sediment loads.

One clear caveat to the evidence for increased terrigenous fluxes across the T-OAE is that there are few data on actual changes in clastic sedimentation rates. Quantitative constraints on sedimentation rates across the T-OAE are rare due to the debated timescale of the NCIE and a paucity of robust temporal constraints (radioisotopic or cyclostratigraphic) across the early Toarcian as a whole (Hesselbo et al., 2020, though see Kemp et al., 2024 for a recent high-precision U—Pb geochronology study that constrained the NCIE to <407 kyr). This contrasts with the CPE and PETM, where order-of-magnitude increases in clastic sedimentation rates to be calculated across multiple basins

(both tropical and temperate) (John et al., 2008; Jin et al., 2022a; Dal Corso et al., 2024).

Although calculation of changes in sedimentation rates through the NCIE has not been done, there is clear evidence from deep water and anoxic-euxinic sections in northwest Europe that the NCIE interval is often condensed (e.g., Kemp et al., 2022). Ostensibly, such condensation could be attributable to a reduction in terrigenous detrital fluxes linked to weakened hydrological cycling and runoff. In the relatively deep-water Skladaná Skala (Slovakia) section, for example, a reduced input of siliciclastic detritus is inferred based on the extremely low thickness (~1 m) of the NCIE there (Müller et al., 2020). Müller et al. (2020) noted how the inference of reduced terrigenous flux at Skladaná Skala is at odds with the widespread evidence for increased fluxes in shallower and more proximal sites. As such, the observed condensation can more reasonably be attributed to the known sea level rise and/or fall in hemipelagic carbonate production during the T-OAE (Müller et al., 2020 and references therein). Under these circumstances, enhanced terrigenous supply during warming was not sufficient to compensate for the reduced deep-water sediment fluxes caused by the coeval effects of reduced carbonate production and transgression (Müller et al., 2020). The crisis in carbonate production that characterised the T-OAE likely impacts interpretation of terrigenous flux changes in shallower platform/ramp sections. For example, at La Cerradura (Spain), Breggia (Switzerland) and Cuers (France), the relative increase in siliciclastic flux during the NCIE can be linked at least in part to low rates of carbonate production rather than increased terrigenous fluxes (Léonide et al., 2012; Reolid et al., 2014; Fantasia et al., 2018a).

In anoxic-euxinic basins in northwest Europe, previous work has noted how prasinophyte algae and amorphous organic matter (characterised by high hydrogen index values) can dominate in the NCIE relative to terrestrial organic matter (characterised by low hydrogen index values) (Suan et al., 2015 and references therein). This phenomenon is unlikely to be linked to a reduction in terrigenous organic matter flux, however, and instead can be attributed to enhanced preservation of amorphous organic matter under anoxic conditions (Suan et al., 2015). Anoxic sites with elevated hydrogen index within the NCIE (e.g. Dotterhausen, Denkingen, Yorkshire, Kelimyar River, Polovinnaya River; Table 1) are thus not interpreted as providing evidence for terrigenous flux change in this study (see Table S1).

Overall, inferred increases in physical and chemical weathering and terrigenous fluxes are recorded globally during the NCIE. It is likely that these increases were associated with increased frequency and intensity of extreme precipitation. Climate models and modern observations support this inference, as well as the possibility that storms could have been responsible for delivering much of the inferred extreme precipitation (e.g., IPCC, 2023, see also Guzman and Jiang, 2021). This latter inference is fully consistent with the evidence for enhanced storm activity during the NCIE (Section 4.1).

### 4.4. Salinity changes as a hydroclimate indicator during the T-OAE NCIE

An important predicted consequence of accelerated freshwater runoff inferred in Section 4.3 above is a reduction of surface water salinity in marginal seas, and potentially water column stratification in both marginal seas and lakes. Early work in Northern Europe noted that a reduction in oxygen isotope ($\delta^{18}O$) values in fossil marine belemnites across the NCIE were likely too extreme to be due to seawater warming alone, and it was suggested that influx of freshwater (with relatively low $\delta^{18}O$) could have contributed to the observed changes (Schmid-Röhl et al., 2002; Bailey et al., 2003; Rosales et al., 2004). This rather indirect evidence for salinity reduction has subsequently been augmented with palynological and geochemical evidence. In particular, the abundance of freshwater-tolerant nannofossil taxa (e.g., *Calyculus* nannoplankton, Mattioli et al., 2004, 2008), and organic and inorganic geochemical proxies (methylated methyl trimethyltridecylchromane abundance, and B/Ga ratios) (e.g., Ruebsam et al., 2018; Remírez and Algeo, 2020). Salinity changes are of specific interest at the T-OAE because of: 1) the possible role played by the combined effects of runoff of nutrients and salinity stratification in triggering and sustaining anoxia (e.g., Farrimond et al., 1989), and 2) the possibility that freshwater fluxes originated at least partly from melting of high latitude ice due to warming (Ruebsam et al., 2019).

In our compilation, 22 sites record weak or strong evidence for reduced salinity waters or water column stratification across the NCIE (Table 1, Fig. 7). No sites record an increase in salinity during the NCIE, despite the evidence for sea level rise and the consequent effect this might be expected to have on freshwater influence from rivers. The evidence for reduced salinity across the T-OAE is mainly recorded in Europe (as expected given the preponderance of European sites). In detail, much of the evidence is concentrated in Northern Europe at sites where organic matter enrichment and deoxygenation were strongest (Fig. 7), potentially supporting a possible link between salinity stratification and deoxygenation (Farrimond et al., 1989). Nevertheless, the compilation is almost certainly biased by the tendency for such sites to be the paleontologically and geochemically well-studied. In particular, the conditions at these sites (fine-grained, oxygen-deficient) were favourable to the preservation of nannofossils useful as paleosalinity proxies, such as freshwater-tolerant *Calyculus* taxa. The high total organic carbon (TOC) content of the rocks has also made them the subject of organic geochemical studies, which can also yield data potentially indicative of salinity changes and/or water column stratification (e.g., Farrimond et al., 1989; Ruebsam et al., 2018). In detail, therefore, no clear link can yet be made between deoxygenation across the T-OAE and freshwater runoff. We note, for instance, that evidence for reduced surface water salinity is not restricted to anoxic-euxinic sites with high TOC (Fig. 7). Notably, well-oxygenated and organic-poor sites such as Peniche and Pozzale also show reduced surface water salinity (Fig. 7; see Kemp et al., 2022 for details of redox conditions at these and other sites).

The geographic pattern of the salinity data provides no clear support for the hypothesis that T-OAE salinity changes in Europe were driven by low salinity water flowing from high latitudes through the Viking Corridor, as suggested by Prauss and Riegel (1989) and Ruebsam et al. (2019), and supported by climate modelling work by Dera and Donnadieu (2012) (Fig. 7). Separately, van de Schootbrugge et al. (2019) challenged the idea of significant meltwater outflow given the lack of evidence for salinity reduction across the NCIE within the Viking Corridor at the 34/10–35 site in Norway (Fig. 2; also known as Gulfaks). Water column stratification or enhanced freshwater runoff has also been inferred in Chinese lacustrine basins, such as Sichuan Basin (Core A and LQ104X sites, Xu et al., 2021; Liu et al., 2022a) (Fig. 7).

Our compilation suggests that salinity reduction in marine waters and water column stratification in both marine and lacustrine basins across the NCIE was facilitated by widespread freshwater inputs controlled by enhanced runoff. Just over half of all sites where weak or strong evidence of salinity reduction/stratification occurs across the NCIE also contain evidence of enhanced terrigenous inputs and/or enhanced weathering (Table 1). However, compared to data on terrigenous inputs and weathering, data on salinity changes across the NCIE are sparse, and continued application of novel geochemical proxies (such as the recently-developed B/Ga proxy, Wei and Algeo, 2019) is needed to more fully establish the precise geographic pattern and scale of freshwater inputs, particularly outside of Europe. Such data are also needed to further evaluate the potential causal links between salinity changes and anoxia.

## 5. Synopsis and conclusions

Our analysis of data from 109 globally distributed and mainly shallow marine sites demonstrates that marked changes in hydroclimate occurred in response to carbon release and global warming at the T-OAE. The data support the broad inference that warming drove an

intensification in hydrological cycling; involving extreme precipitation, increased weathering and freshwater runoff, enhanced terrigenous fluxes to marine and non-marine basins, intensified and geographically widespread tropical cyclone activity, and enhanced turbidity current generation triggered by storms and/or enhanced terrigenous fluxes. Only rarely do the studied T-OAE sites provide evidence for reduced hydrological cycling and increased aridity.

Despite this overarching finding, our work also underlines that care is needed when interpreting the available data. As noted in Section 2, geological interpretation of data that can be used to infer hydroclimate changes can be ambiguous. In particular, the occurrence of abundant turbidites across the T-OAE that we document at some sites could, at least in some cases, be due to non-climatic factors (i.e. tectonics). Similarly, further data on salinity changes across the T-OAE are needed before definitive inferences regarding the significance of enhanced freshwater runoff can be made. A separate key issue with the evidence we present is that the data themselves are likely to be biased. Of particular note is that T-OAE records from continental interior regions are rare, and at least some continental interior regions could have been associated with enhanced aridity during warming (Dera and Donnadieu, 2012). A second caveat is that the sedimentary record itself is likely biased toward preserving strata deposited during wetter conditions, since this is when basins and sediment routing systems reach geographic (and perhaps sediment load) maxima, and hence when sedimentary records of the event are most likely to be deposited and preserved. On this latter point, it is also important to reiterate that the hydroclimatic significance of the observed increase in terrigenous fluxes across the T-OAE is potentially ambiguous, and on its own does not necessarily imply a wetter climate (e.g., Syvitski and Milliman, 2007). However, the separate evidence for increased weathering and reduced salinity at many sites provides support for the inference that terrigenous fluxes increased because of enhanced sediment mobilisation and runoff caused by higher fluvial discharge rates under overall wetter conditions.

A stand-out feature of the compilation is the widespread evidence for intensified storm activity across the T-OAE NCIE. Importantly, these data support predictions made about future storm behaviour in response to increasing anthropogenic $CO_2$ emissions, including: 1) an overall increase in the frequency of intense tropical cyclones, 2) a poleward expansion of tropical cyclones, and/or 3) a possible increase in the intensity of extratropical storms. By contrast, we note that there is comparatively little evidence for intensified storm activity during other hyperthermal events such as the PETM, CPE and Permian-Triassic mass extinction, all of which were characterised by $CO_2$ rise and global warming. For the PETM in particular, which was likely genetically and paleoclimatically similar to the T-OAE (e.g., Cohen et al., 2007), climate modelling has predicted intensification and poleward expansion of tropical cyclones in response to rising $CO_2$ and temperature (e.g., Kiehl et al., 2021; Studholme et al., 2021). However, geological evidence to support this modelling is sparse (Li et al., 2021; see also Jiang et al., 2022). Similarly, the CPE is the only deep time hyperthermal named for its hydroclimatic significance, with clear evidence of large-scale increases in terrigenous fluxes (e.g., Dal Corso et al., 2024). However, to our knowledge no evidence has been presented for an increase in storm deposits during the CPE. This leads to the question of whether storm deposits have been sufficiently searched for in records of these other hyperthermals. Regardless, the T-OAE likely serves as the best deep time analogue for the extreme weather system changes predicted for Earth's future.

A great deal of T-OAE work to date has concentrated on understanding and documenting redox changes and the cause(s) of the event, with the hydroclimate significance of the T-OAE only more recently being appreciated. Recent work has suggested that the importance of anoxia as a characteristic of the T-OAE may be somewhat overstated (see for example, McArthur, 2019). A recent review by Kemp et al. (2022) suggested that ~69 % of T-OAE sites (46 out of 67) showed evidence for appreciable deoxygenation (i.e. development of at least suboxic-anoxic conditions). In our work, we have shown that a comparable proportion of sites (~63 %, 69 out of 109) show evidence for hydroclimate change that can be linked to an enhancement of the hydrological cycle. In this respect, then, hydroclimate change was perhaps as much of a defining feature of the T-OAE as deoxygenation.

## Declaration of competing interest

The authors declare that they have no known competing financial interests or personal relationships that could have appeared to influence the work reported in this paper.

## Data availability

Data will be made available on request.

## Acknowledgements

This research was financially supported by the National Natural Science Foundation of China (NSFC grants 42488201, 41888101 and 42272033), and the National Key Research and Development Program of China (grant 2023YFF0804000). The research of VB is conducted in the scope of the internal research project "WEGETA" at the Croatian Geological Survey, funded by the National Recovery and Resilience Plan 2021–2026 of the European Union – NextGenerationEU, and monitored by the Ministry of Science and Education of the Republic of Croatia. The work is a contribution to IGCP 739.

## Appendix A. Supplementary data

Supplementary data to this article can be found online at https://doi.org/10.1016/j.earscirev.2024.104946.

## References

Algeo, T.J., Twitchett, R.J., 2010. Anomalous early Triassic sediment fluxes due to elevated weathering rates and their biological consequences. Geology 38, 1023–1026.

Al-Hussaini, A., Alnazghah, M., Al-Ramadan, K., Fallatah, M., Polo, C., 2021. Asymmetrical wave-dominated siliciclastic shorelines with evidence of along-strike variability of sedimentary processes: a revised interpretation for the Toarcian Marrat red beds, Central Arabia. Mar. Pet. Geol. 126, 104915.

Alnazghah, M., Koeshidayatullah, A., Al-Hussaini, A., Amao, A., Song, H., Al-Ramadan, K., 2022. Evidence for the early Toarcian Carbon Isotope Excursion (T-CIE) from the shallow marine siliciclastic red beds of Arabia. Sci. Rep. 12, 18124. https://doi.org/10.1038/s41598-022-21716-0.

Al-Suwaidi, A.H., Angelozzi, G.N., Baudin, F., Damborenea, S.E., Hesselbo, S.P., Jenkyns, H.C., Manceñido, M.O., Riccardi, A.C., 2010. First record of the early Toarcian oceanic anoxic event from the Southern Hemisphere, Neuquén Basin, Argentina. J. Geol. Soc. Lond. 167 (4), 633–636.

Al-Suwaidi, A., Hesselbo, S.P., Damborenea, S.E., Manceñido, M.O., Jenkyns, H.C., Riccardi, A.C., Angelozzi, G.N., Baudin, F., 2016. The Toarcian Oceanic Anoxic Event (early Jurassic) in the Neuquén Basin, Argentina: a Reassessment of Age and Carbon Isotope Stratigraphy. J. Geol. 124, 171–193.

Asgar-Deen, M., Hall, R., Craig, J., Riediger, C., 2003. New biostratigraphic data from the lower Jurassic Fernie Formation in the subsurface of west-Central Alberta and their stratigraphic implications. Can. J. Earth Sci. 40, 45–63.

Bailey, T.R., Rosenthal, Y., McArthur, J.M., van de Schootbrugge, B., Thirlwall, M.F., 2003. Paleoceanographic changes of the Late Pliensbachian–Early Toarcian interval: a possible link to the genesis of an Oceanic Anoxic Event. Earth Planet. Sci. Lett. 212 (3–4), 307–320.

Bailey, L.P., Clare, M.A., Rosenberger, K.J., Cartigny, M.J., Talling, P.J., Paull, C.K., Gwiazda, R., Parsons, D.R., Simmons, S.M., Xu, J., Haigh, I.D., Maier, K.L., McGann, M., Lundsten, E., Monterey CCE Team, 2021. Preconditioning by sediment accumulation can produce powerful turbidity currents without major external triggers. Earth Planet. Sci. Lett. 562, 116845.

Baranyi, V., Pálfy, J., Görög, Á., Riding, J.B., Raucsik, B., 2016. Multiphase response of palynomorphs to the Toarcian oceanic anoxic event (early Jurassic) in the Réka Valley section, Hungary. Rev. Palaeobot. Palynol. 235, 51–70.

Baranyi, V., Jin, X., Dal Corso, J., Li, B., Kemp, D.B., 2024. Vegetation response to climate change during an early Jurassic hyperthermal event (Jenkyns Event) from Northern China (Ordos Basin). Palaeogeogr. Palaeoclimatol. Palaeoecol. 643, 112180.

Bellanca, A., Masetti, D., Neri, R., Venezia, F., 1999. Geochemical and sedimentological evidence of productivity cycles recorded in Toarcian black shales from the Belluno Basin, Southern Alps, northern Italy. J. Sediment. Res. 69 (2), 466–472.
Bhatia, K.T., Vecchi, G.A., Knutson, T.R., Murakami, H., Kossin, J., Dixon, K.W., Whitlock, C.E., 2019. Recent increases in tropical cyclone intensification rates. Nat. Commun. 10, 635.
Bodin, S., Mattioli, E., Fröhlich, S., Marshall, J.D., Boutib, L., Lahsini, S., Redfern, J., 2010. Toarcian carbon isotope shifts and nutrient changes from the Northern margin of Gondwana (High Atlas, Morocco, Jurassic): palaeoenvironmental implications. Palaeogeogr. Palaeoclimatol. Palaeoecol. 297 (2), 377–390.
Bodin, S., Fröhlich, S., Boutib, L., Lahsini, S., Redfern, J., 2011. Assessment of early Toarcian source rock potential in the Central High Atlas Basin (Central Morocco): Regional distribution and depositional model. J. Pet. Geol. 34, 345–364.
Bodin, S., Krencker, F.-N., Kothe, T., Hoffmann, R., Mattioli, E., Heimhofer, U., Kabiri, L., 2016. Perturbation of the carbon cycle during the late Pliensbachian - early Toarcian: New insight from high-resolution carbon isotope records in Morocco. J. Afr. Earth Sci. 116, 89–104.
Bomou, B., Suan, G., Schlögel, J., Grosjean, A.-S., Suchéras-Marx, B., Adatte, T., Spangenberg, J.E., Fouché, S., Zacaï, A., Gibert, C., Brazier, J.-M., Perrier, P., Vincent, P., Janneau, K., Martin, J.E., 2021. The paleoenvironmental context of Toarcian vertebrate-yielding shales of southern France (Hérault). Geol. Soc. Lond. Spec. Publ. 514, 121–152.
Boulila, S., Galbrun, B., Sadki, D., Gardin, S., Bartolini, A., 2019. Constraints on the duration of the early Toarcian T-OAE and evidence for carbon-reservoir change from the High Atlas (Morocco). Glob. Planet. Chang. 175, 113–128.
Brański, P., 2010. Kaolinite peaks in early Toarcian profiles from the Polish Basin – an inferred record of global warming. Geol. Quart. 54 (1), 15–24.
Brański, P., 2012. The mineralogical record of the early Toarcian stepwise climate changes and other environmental variations (Ciechocinek Formation, Polish Basin). Volumina Jurassica 10 (1), 1–24.
Brazier, J.M., Suan, G., Tacail, T., Simon, L., Martin, J.E., Mattioli, E., Balter, V., 2015. Calcium isotope evidence for dramatic increase of continental weathering during the Toarcian oceanic anoxic event (early Jurassic). Earth Planet. Sci. Lett. 411, 164–176.
Cao, Y., Song, H., Algeo, T.J., Chu, D., Du, Y., Tian, L., Wang, Y., Tong, J., 2019. Intensified chemical weathering during the Permian-Triassic transition recorded in terrestrial and marine successions. Palaeogeogr. Palaeoclimatol. Palaeoecol. 519, 166–177.
Carmichael, M.J., Inglis, G.N., Badger, M.P., Naafs, B.D.A., Behrooz, L., Remmelzwaal, S., Pancost, R.D., 2017. Hydrological and associated biogeochemical consequences of rapid global warming during the Paleocene–Eocene Thermal Maximum. Glob. Planet. Chang. 157, 114–138.
Carmichael, M.J., Pancost, R.D., Lunt, D.J., 2018. Changes in the occurrence of extreme precipitation events at the Paleocene–Eocene thermal maximum. Earth Planet. Sci. Lett. 501, 24–36.
Caruthers, A.H., Gröcke, D.R., Smith, P.L., 2011. The significance of an early Jurassic (Toarcian) carbon-isotope excursion in Haida Gwaii (Queen Charlotte Islands), British Columbia, Canada. Earth Planet. Sci. Lett. 307, 19–26.
Chapman, W.A.L., Finnegan, N.J., 2024. The signature of climate in fluvial suspended sediment records. J. Geophys. Res. Earth 129, e2023JF007429.
Chen, W., Kemp, D.B., He, T., Huang, C., Jin, S., Xiong, Y., Newton, R.J., 2021. First record of the early Toarcian Oceanic Anoxic Event in the Hebrides Basin (UK) and implications for redox and weathering changes. Glob. Planet. Chang. 207, 103685.
Chen, W., Kemp, D.B., He, T., Newton, R.J., Xiong, Y., Jenkyns, H.C., Izumi, K., Cho, T., Huang, C., Poulton, S.W., 2023a. Shallow- and deep-ocean Fe cycling and redox evolution across the Pliensbachian–Toarcian boundary and Toarcian Oceanic Anoxic Event in Panthalassa. Earth Planet. Sci. Lett. 602, 117959.
Chen, P., Xian, B., Li, M., Fang, M., Ur Rahman, N., Liu, J., Chen, S., Tian, R., Wu, W., 2023b. Intensified lacustrine turbidite deposition as a response to the Carnian Pluvial Episode: Insights from the Triassic Ordos Basin in North China Plate. Palaeogeogr. Palaeoclimatol. Palaeoecol. 623, 111599.
Clare, M.A., Talling, P.J., Hunt, J.E., 2015. Implications of reduced turbidity current and landslide activity for the initial Eocene thermal Maximum–evidence from two distal, deep-water sites. Earth Planet. Sci. Lett. 420, 102–115.
Clémence, M.-E., Gardin, S., Bartolini, A., 2015. New insights in the pattern and timing of the early Jurassic calcareous nannofossil crisis. Palaeogeogr. Palaeoclimatol. Palaeoecol. 427, 100–108.
Cohen, A.S., Coe, A.L., Harding, S.M., Schwark, L., 2004. Osmium isotope evidence for the regulation of atmospheric $CO_2$ by continental weathering. Geology 32, 157–160.
Cohen, A.S., Coe, A.L., Kemp, D.B., 2007. The Late Palaeocene–Early Eocene and Toarcian (Early Jurassic) carbon isotope excursions: a comparison of their time scales, associated environmental changes, causes and consequences. J. Geol. Soc. Lond. 164, 1093–1108.
Correia, V.F., Riding, J.B., Duarte, L.V., Fernandes, P., Pereira, Z., 2017. The palynological response to the Toarcian Oceanic Anoxic Event (early Jurassic) at Peniche, Lusitanian Basin, western Portugal. Mar. Micropaleontol. 137, 46–63.
Cui, H., Zhu, S., Liang, C., Ma, W., Tong, H., Shi, Z., 2023. Facies association analysis of a Toarcian siliciclastic-carbonate lacustrine system, Sichuan Basin, China. Palaeogeogr. Palaeoclimatol. Palaeoecol. 631, 111841.
Dal Corso, J., Sun, Y., Kemp, D.B., 2024. Palaeogeographic heterogeneity of large-amplitude changes in marine sedimentation rates during the Carnian Pluvial Episode (Late Triassic). Glob. Planet. Chang. 237, 104437.
Deng, S.H., Lu, Y.Z., Fan, R., Fang, L.H., Li, X., Liu, L., 2012. Toarcian (early Jurassic) oceanic anoxic event and the responses in terrestrial ecological system. Earth Sci. J. China Univ. Geosci. 37, 23–38 (in Chinese with English abstract).
Deng, S.H., Yang, X., Lu, Y., Sha, J., 2024. A thermophilous and arid-tolerant flora from the Lower Jurassic of the Junggar Basin, Xinjang, NW China, corresponding to the Toarcian Oceanic Anoxic Event, Geological Society of London Special Publication, vol. 538, pp. 179–210.
Dera, G., Donnadieu, Y., 2012. Modeling evidences for global warming, Arctic seawater freshening, and sluggish oceanic circulation during the early Toarcian anoxic event. Paleoceanography 27, PA211.
Dera, G., Pellenard, P., Neige, P., Deconinck, J.F., Pucéat, E., Dommergues, J.L., 2009. Distribution of clay minerals in early Jurassic Peritethyan seas: palaeoclimatic significance inferred from multiproxy comparisons. Palaeogeogr. Palaeoclimatol. Palaeoecol. 271 (1–2), 39–51.
Dosseto, A., Vigier, N., Joannes-Boyau, R., Moffat, I., Singh, T., Srivastava, P., 2015. Rapid response of silicate weathering rates to climate change in the Himalaya. Geochem. Perspect. Lett. 1, 10–19.
Duarte, L.V., 2007. Lithostratigraphy, sequence stratigraphy and depositional setting of the Pliensbachian and Toarcian series in the Lusitanian Basin, Portugal. In: Rocha, R. B. (Ed.), The Peniche Section (Portugal). Contributions to the Definition of the Toarcian GSSP. International Subcommission on Jurassic Stratigraphy, pp. 17–23.
Duarte, L.V., Soares, A.F., 2002. Litostratierafia das series marso-calcírias do Jurássico inferior da Bacia Lusitànica (Portugal). Commun. Inst. Geol. Mineiro 89, 135–154.
Duarte, L.V., Oliveira, L.C., Rodrigues, R., 2007. Carbon isotopes as a sequence stratigraphic tool: examples from the lower and Middle Toarcian marly limestones of Portugal. Geol. Minero 118, 3–18.
Elsner, J., Kossin, J., Jagger, T., 2008. The increasing intensity of the strongest tropical cyclones. Nature 455, 92–95.
Emanuel, K., 2005. Increasing destructiveness of tropical cyclones over the past 30 years. Nature 436, 686–688.
Emanuel, K., 2008. The Hurricane-climate connection. Bull. Am. Meteorol. Soc. 101 (3), E303–E322.
Erba, E., Cavalheiro, L., Dickson, A.J., Faucher, G., Gambacorta, G., Jenkyns, H.C., Wagner, T., 2022. Carbon- and oxygen-isotope signature of the Toarcian Oceanic Anoxic Event: insights from two Tethyan pelagic sequences (Gajum and Sogno Cores – Lombardy Basin, northern Italy). Newsl. Stratigr. 55 (4). https://doi.org/10.1127/nos/2022/0690.
Ettinger, N.P., Larson, T.E., Kerans, C., Thibodeau, A., Hattori, K.E., Kacur, S.M., Martindale, R.C., 2021. Ocean acidification and photic-zone anoxia at the Toarcian Oceanic Anoxic Event: Insights from the Adriatic Carbonate Platform. Sedimentology 68, 63–107.
Fantasia, A., Föllmi, K.B., Adatte, T., Spangenberg, J.E., Montero-Serrano, J.C., 2018a. The early Toarcian oceanic anoxic event: Paleoenvironmental and paleoclimatic change across the Alpine Tethys (Switzerland). Glob. Planet. Chang. 162, 53–68.
Fantasia, A., Föllmi, K.B., Adatte, T., Bernárdez, E., Spangenberg, J.E., Mattioli, E., 2018b. The Toarcian Oceanic Anoxic Event in southwestern Gondwana: an example from the Andean Basin, northern Chile. J. Geol. Soc. Lond. 175, 883–902.
Fantasia, A., Föllmi, K.B., Adatte, T., Spangenberg, J.E., Mattioli, E., 2019a. Expression of the Toarcian Oceanic Anoxic Event: New insights from a Swiss transect. Sedimentology 66, 262–284.
Fantasia, A., Adatte, T., Spangenberg, J.E., Font, E., Duarte, L.V., Föllmi, K.B., 2019b. Global versus local processes during the Pliensbachian-Toarcian transition at the Peniche GSSP, Portugal: A multi-proxy record. Earth Sci. Rev. 102932.
Farrimond, P., Eglington, G., Brassell, S.G., Jenkyns, H.C., 1989. Toarcian oceanic anoxic event in Europe: an organic geochemical study. Mar. Pet. Geol. 6, 136–147.
Fernández-Martínez, J., Rodríguez-Tovar, F.J., Piñuela, L., Martínez-Ruiz, F., García-Ramos, J.C., 2021. Bottom- and pore-water oxygenation during the early Toarcian Oceanic Anoxic Event (T-OAE) in the Asturian Basin (N Spain): Ichnological information to improve facies analysis. Sediment. Geol. 419. https://doi.org/10.1016/j.sedgeo.2021.105909.
Fonseca, C., Mendonça Filho, J.G., Lézin, C., Duarte, L.V., Fauré, P., 2018. Organic facies variability during the Toarcian Oceanic Anoxic event record of the Grands causes and Quercy basins (southern France). Int. J. Coal Geol. 190, 218–235.
Font, E., Duarte, L.V., Dekkers, M.J., Remazeilles, C., Egli, R., Spangenberg, J.E., Fantasia, A., Ribeiro, J., Gomes, E., Mirão, J., Adatte, T., 2022. Rapid light carbon releases and increased aridity linked to Karoo–Ferrar magmatism during the early Toarcian oceanic anoxic event. Sci. Rep. 12, 4342. https://doi.org/10.1038/s41598-022-08269-y.
Fu, X.G., Tan, F., Feng, X., Wang, D., Chen, W., Song, C., Zeng, S., 2014. Early Jurassic anoxic conditions and organic accumulation in the eastern Tethys. Int. Geol. Rev. 56 (12), 1450–1465.
Fu, X.G., Wang, J., Feng, X., Wang, D., Chen, W., Song, C., Zeng, S., 2016. Early Jurassic carbon-isotope excursion in the Qiangtang Basin (Tibet), the eastern Tethys: implications for the Toarcian Oceanic anoxic event. Chem. Geol. 442, 62–72.
Fürisch, F., Berndt, R., Scheuer, T., Gahr, M., 2001. Comparative ecological analysis of Toarcian (lower Jurassic) benthic faunas from southern France and east-Central Spain. Lethaia 34, 169–199.
Gahr, M.E., 2005. Response of lower Toarcian (lower Jurassic) macrobenthos of the Iberian Peninsula to sea level changes and mass extinction. J. Iber. Geol. 31 (2), 197–215.
Gambacorta, G., Cavalheiro, L., Brumsack, H.-J., Dickson, A.J., Jenkyns, H.C., Schnetger, B., Wagner, T., Erba, E., 2023. Suboxic conditions prevailed during the Toarcian Oceanic Anoxic Event in the Alpine-Mediterranean Tethys: the Sogno Core pelagic record (Lombardy Basin, northern Italy). Glob. Planet. Chang. 223, 104089.
Ghadeer, S.G., Macquaker, J.H.S., 2011. Sediment transport processes in an ancient mud-dominated succession: a comparison of processes operating in marine offshore settings and anoxic basinal environments. J. Geol. Soc. Lond. 168, 835–846.
Ghadeer, S.G., Macquaker, J.H.S., 2012. The role of event beds in the preservation of organic carbon in finegrained sediments: analyses of the sedimentological processes operating during deposition of the Whitby Mudstone Formation (Toarcian, lower Jurassic) preserved in Northeast England. Mar. Pet. Geol. 35, 309–320.

Gómez, J.J., Goy, A., Canales, M.L., 2008. Seawater temperature and carbon isotope variations in belemnites linked to mass extinction during the Toarcian (early Jurassic) in Central and Northern Spain. Comparisons with other European sections. Palaeogeogr. Palaeoclimatol. Palaeoecol. 258, 28–58.
Gray, W.M., 1968. Global view of the origin of tropical disturbances and storms. Mon. Weather Rev. 96, 669–700.
Guzman, O., Jiang, H., 2021. Global increase in tropical cyclone rain rate. Nat. Commun. 12, 5344.
Hallam, A., 2001. A review of the broad pattern of Jurassic Sea-level changes and their possible causes in the light of current knowledge. Palaeogeogr. Palaeoclimatol. Palaeoecol. 167, 23–37.
Han, Z., Hu, X., Kemp, D.B., Li, J., 2018. Carbonate-platform response to the Toarcian Oceanic Anoxic Event in the southern hemisphere: Implications for climatic change and biotic platform demise. Earth Planet. Sci. Lett. 489, 59–71.
Han, Z., Hu, X., Hu, Z., Jenkyns, H.C., Su, T., 2022. Geochemical evidence from the Kioto Carbonate Platform (Tibet) reveals enhanced terrigenous input and deoxygenation during the early Toarcian. Glob. Planet. Chang. 215, 103887.
Hermoso, M., Pellenard, P., 2014. Continental weathering and climatic changes inferred from clay mineralogy and paired carbon isotopes across the early to middle Toarcian in the Paris Basin. Palaeogeogr. Palaeoclimatol. Palaeoecol. 399, 385–393.
Hermoso, M., Minoletti, F., Pellenard, P., 2013. Black shale deposition during Toarcian super-greenhouse driven by sea level. Clim. Past 9, 2703–2712.
Hesselbo, S.P., 2008. Sequence stratigraphy and inferred relative sea-level change from the onshore British Jurassic. Proc. Geol. Assoc. 119, 19–34.
Hesselbo, S.P., Pieńkowski, G., 2011. Stepwise atmospheric carbon-isotope excursion during the Toarcian Oceanic Anoxic Event (early Jurassic, Polish Basin). Earth Planet. Sci. Lett. 301, 365–372.
Hesselbo, S.P., Gröcke, D.R., Jenkyns, H.C., Bjerrum, C.J., Farrimond, P., Bell, H.S.M., Green, O.R., 2000. Massive dissociation of gas hydrate during a Jurassic oceanic anoxic event. Nature 406, 392–395.
Hesselbo, S.P., Jenkyns, H.C., Duarte, L.V., Oliveira, L.C., 2007. Carbon-isotope record of the early Jurassic (Toarcian) Oceanic Anoxic event from fossil wood and marine carbonate (Lusitanian Basin, Portugal). Earth Planet. Sci. Lett. 253 (3–4), 455–470.
Hesselbo, S.P., Ogg, J.G., Ruhl, M., 2020. The Jurassic Period. In: Gradstein, F.M., Ogg, J. G., Schmitz, M.D., Ogg, G.M. (Eds.), Geologic Time Scale 2020. Elsevier, pp. 955–1021.
Hirabayashi, Y., Mahendran, R., Koirala, S., Konoshima, L., Yamazaki, D., Watanabe, S., Kim, H., Kanae, S., 2013. Global flood risk under climate change. Nat. Clim. Chang. 3, 816–821.
Houben, A.J.P., Goldberg, T., Slomp, C.P., 2021. Biogeochemical evolution and organic carbon deposition on the Northwestern European Shelf during the Toarcian Ocean Anoxic Event. Palaeogeogr. Palaeoclimatol. Palaeoecol. 565, 110191.
Hougård, I.W., Bojesen-Koefoed, J.A., Vickers, M.L., Ullmann, C.V., Bjerrum, C.J., Rizzi, M., Korte, C., 2021. Redox element record shows that environmental perturbations associated with the T-OAE were of longer duration than the carbon isotope record suggests – the Aubach section, SW Germany. Newsl. Stratigr. 54 (2). https://doi.org/10.1127/nos/2020/0630.
Ikeda, M., Hori, R.S., Ikehara, M., Miyashita, R., Chino, M., Yamada, K., 2018. Carbon cycle dynamics linked with Karoo-Ferrar volcanism and astronomical cycles during Pliensbachian-Toarcian (early Jurassic). Glob. Planet. Chang. 170, 163–171.
IPCC, 2023. Climate Change 2021 – The Physical Science Basis: Working Group I Contribution to the Sixth Assessment Report of the Intergovernmental Panel on Climate Change. Cambridge University Press, Cambridge, 2391 pp.
Izumi, K., Endo, K., Kemp, D.B., Inui, M., 2018. Oceanic redox conditions through the late Pliensbachian to early Toarcian on the northwestern Panthalassa margin: Insights from pyrite and geochemical data. Palaeogeogr. Palaeoclimatol. Palaeoecol. 493, 1–10.
Jenkyns, H.C., 1988. The early Toarcian (Jurassic) Anoxic Event – stratigraphic, sedimentary, and geochemical evidence. Am. J. Sci. 288, 101–151.
Jenkyns, H.C., Clayton, C.J., 1997. Lower Jurassic epicontinental carbonates and mudstones from England and Wales: chemostratigraphic signals and the early Toarcian anoxic event. Sedimentology 44, 687–706.
Jenkyns, H.C., Gröcke, D.R., Hesselbo, S.P., 2001. Nitrogen isotope evidence for water mass denitrification during the early Toarcian (Jurassic) oceanic anoxic event. Paleoceanography 16 (6), 593–603.
Jiang, J., Hu, X., Garzanti, E., Li, J., BouDagher-Fadel, M.K., Sun, G., Xu, Y., 2022. Enhanced storm–induced turbiditic events during early Paleogene hyperthermals (Arabian continental margin, SW Iran). Glob. Planet. Chang. 214, 103832.
Jin, S., Kemp, D.B., Jolley, D.W., Viera, M., Zachos, J.C., Huang, C., Li, M., Chen, W., 2022a. Large-scale, astronomically-controlled sediment input to the North Sea Basin during the Paleocene Eocene thermal Maximum. Earth Planet. Sci. Lett. 579, 117340.
Jin, X., Zhang, F., Baranyi, V., Kemp, D.B., Feng, X., Grasby, S.E., Sun, G., Shi, Z., Chen, W., Dal Corso, J., 2022b. Early Jurassic massive release of terrestrial mercury linked to floral crisis. Earth Planet. Sc. Lett. 598, 117842. https://doi.org/10.1016/j epsl.2022.117842.
John, C.M., Bohaty, S.M., Zachos, J.C., Sluijs, A., Gibbs, S., Brinkhuis, H., Bralower, T.J., 2008. North American continental margin records of the Paleocene-Eocene thermal maximum: Implications for global carbon and hydrological cycling. Paleoceanography 23, PA2217.
Kafousia, N., Karakitsios, V., Jenkyns, H.C., Mattioli, E., 2011. A global event with a regional character: the early Toarcian Oceanic Anoxic Event in the Pindos Ocean (northern Peloponnese, Greece). Geol. Mag. 148 (4), 619–631.
Kafousia, N., Karakitsios, V., Mattioli, E., Kenjo, S., Jenkyns, H.C., 2014. The Toarcian Oceanic Anoxic Event in the Ionian Zone, Greece. Palaeogeogr. Palaeoclimatol. Palaeoecol. 393, 135–145.
Kemp, D.B., Izumi, K., 2014. Multiproxy geochemical analysis of a Panthalassic margin record of the early Toarcian oceanic anoxic event (Toyora area, Japan). Palaeogeogr. Palaeoclimatol. Palaeoecol. 414, 332–341.
Kemp, D.B., Coe, A.L., Cohen, A.S., Schwark, L., 2005. Astronomical pacing of methane release in the early Jurassic period. Nature 437, 396–399.
Kemp, D.B., Baranyi, V., Izumi, K., Burgess, R.D., 2019. Organic matter variations and links to climate across the early Toarcian oceanic anoxic event (T-OAE) in Toyora area, Southwest Japan. Palaeogeogr. Palaeoclimatol. Palaeoecol. 530, 90–102.
Kemp, D.B., Sadler, P.M., Vanacker, V., 2020a. The human impact on north American erosion, sediment transfer and storage in a geologic context. Nat. Commun. 11, 6012.
Kemp, D.B., Selby, D., Izumi, K., 2020b. Direct coupling between carbon release and weathering during the Toarcian oceanic anoxic event. Geology 48 (10), 976–980.
Kemp, D.B., Suan, G., Fantasia, A., Jin, S., Chen, W., 2022. Global organic carbon burial during the early Toarcian oceanic anoxic event: patterns and controls. Earth Sci. Rev. 231, 104086.
Kemp, D.B., Ramezani, J., Izumi, K., Al-Suwaidi, A., Huang, C., Chen, W., Zhu, Y., 2024. The timing and duration of large-scale carbon release in the early Jurassic. Geology. https://doi.org/10.1130/G52457.1.
Kiehl, J.T., Zarzycki, C.M., Shields, C.A., Rothstein, M.V., 2021. Simulated changes to tropical cyclones across the Paleocene–Eocene Thermal Maximum (PETM) boundary. Paleogeogr. Paleoclimatol. Palaeoecol. 572, 110421.
Knutson, T., Carmago, S.J., Chan, J.C.L., Emanuel, K., Ho, C.-H., Kossin, J., Mohapatra, M., Satoh, M., Sugi, M., Walsh, K., Wu, L., 2020. Tropical Cyclones and climate Change Assessment: Part II. Projected Response to Anthropogenic Warming. Bull. Am. Meteorol. Soc. 101 (3), E303–E322.
Korty, R.L., Emanuel, K.A., Huber, M., Zamora, R.A., 2017. Tropical cyclones downscaled from simulations with very high carbon dioxide levels. J. Clim. 30, 649–667.
Krencker, F.N., Bodin, S., Suan, G., Heimhofer, U., Kabiri, L., Immenhauser, A., 2015. Toarcian extreme warmth led to tropical cyclone intensification. Earth Planet. Sci. Lett. 425, 120–130.
Krencker, F.-N., Fantasia, A., Danisch, J., Martindale, R., Kabiri, L., El Ouali, M., Bodin, S., 2020. Two-phased collapse of the shallow-water carbonate factory during the late Pliensbachian–Toarcian driven by changing climate and enhanced continental weathering in the Northwestern Gondwana Margin. Earth Sci. Rev. 208, 103254.
Krencker, F.-N., Fantasia, A., El Ouali, M., Kabiri, L., Bodin, S., 2022. The effects of strong sediment-supply variability on the sequence stratigraphic architecture: Insights from early Toarcian carbonate factory collapses. Mar. Pet. Geol. 136, 105469.
Landsea, C.W., Harper, B.A., Hoarau, K., Knaff, J.A., 2006. Climate change. Can we detect trends in extreme tropical cyclones? Science 313 (5786), 452.
Leinfelder, R.R., Schmid, D.U., Nose, M., Werner, W., 2002. Jurassic reef patterns: the expression of a changing globe. In: Kiessling, W. (Ed.), Phanerozoic Reef Patterns. SEPM, pp. 465–520.
Léonide, P., Floquet, M., Durlet, C., Baudin, F., Pittet, B., Lécuyer, C., 2012. Drowning of a carbonate platform as a precursor stage of the early Toarcian global anoxic event (Southern Provence sub-Basin, South-east France). Sedimentology 59, 156–184.
Leonowicz, P., 2011. Sedimentation of lower Toarcian (lower Jurassic) brackish deposits from the Częstochowa-Wieluń region (SW Poland). Acta Geol. Pol. 61 (2), 215–241.
Lézin, C., Andreu, B., Pellenard, P., Bouchez, J.-L., Emmanuel, L., Fauré, P., Landrein, P., 2013. Geochemical disturbance and paleoenvironmental changes during the early Toarcian in NW Europe. Chem. Geol. 341, 1–15.
Li, W., Hu, X., Melinte-Dobrinescu, M.C., BouDagher-Fadel, M., Li, J., Zhang, S., Xu, Y., 2021. Early Paleogene hyperthermal events and their environmental impacts in the Qimugen section, Tarim Sea. Chin. Sci. Bull. 66 (9), 1067–1082 (in Chinese with English abstract).
Li, B., Jin, X., Dal Corso, J., Ogg, J.G., Lang, X., Baranyi, V., Preto, N., Franceschi, M., Qiao, P., Shi, Z., 2023. Complex pattern of environmental changes and organic matter preservation in the NE Ordos lacustrine depositional system (China) during the T-OAE (early Jurassic). Glob. Planet. Chang. 221, 104045.
Liu, J., Cao, J., Hu, G., Wang, Y., Yang, R.F., Liao, Z.W., 2020a. Water-level and redox fluctuations in a Sichuan Basin lacustrine system coincident with the Toarcian OAE. Palaeogeogr. Palaeoclimatol. Palaeoecol. 58, 1–14.
Liu, M., Sun, P., Them, T.R., Li, Y., Sun, S., Gao, X., Huang, X., Tang, Y., 2020b. Organic geochemistry of a lacustrine shale across the Toarcian Oceanic Anoxic Event (early Jurassic) from NE China. Glob. Planet. Chang. 191, 103214.
Liu, J., Cao, J., He, T., Liang, F., Pu, J., Wang, Y., 2022a. Lacustrine redox variations in the Toarcian Sichuan Basin across the Jenkyns Event. Glob. Planet. Chang. 215, 103860.
Liu, R., Hu, G., Cao, J., Yang, R., Liao, Z., Hu, C., Pang, Q., Pang, P., 2022b. Enhanced hydrological cycling and continental weathering during the Jenkyns Event in a lake system in the Sichuan Basin, China. Glob. Planet. Chang. 216, 103915.
Lu, J., Zhou, K., Yang, M., Eley, Y., Shao, L., Hilton, J., 2020. Terrestrial organic carbon isotopic composition (δ13Corg) and environmental perturbations linked to early Jurassic volcanism: evidence from the Qinghai-Tibet Plateau of China. Glob. Planet. Chang. 195, 103331.
Mailliot, S., Mattioli, E., Bartolini, A., Baudin, F., Pittet, B., Guex, J., 2009. Late Pliensbachian-early Toarcian (early Jurassic) environmental changes in an epicontinental basin of NW Europe (Causses area, Central France): a micropaleontological and geochemical approach. Palaeogeogr. Palaeoclimatol. Palaeoecol. 273, 346–364.
Martin, J.E., Suan, G., Suchéras-Marx, B., Rulleau, L., Schlögel, J., Janneau, K., Williams, M., Léna, A., Grosjean, A.-S., Sarroca, E., Perrier, V., Fernandez, V., Charruault, A.-L., Maxwell, E.E., Vincent, P., 2021. Stenopterygiids from the lower Toarcian of Beaujolais and a chemostratigraphic context for ichthyosaur

preservation during the Toarcian Oceanic Anoxic Event. Geol. Soc. Lond. Spec. Publ. 514, 153–172.
Mattioli, E., Pittet, B., 2004. Spatial and temporal distribution of calcareous nannofossils along a proximal–distal transect in the lower Jurassic of the Umbria–Marche Basin (Central Italy). Palaeogeogr. Palaeoclimatol. Palaeoecol. 205, 295–316.
Mattioli, E., Pittet, B., Bucefalo Palliani, R., Röhl, H.J., Schmid-Röhl, A., Morettini, E., 2004. Phytoplankton evidence for the timing and correlation of palaeoceanographical changes during the early Toarcian oceanic anoxic event (early Jurassic). J. Geol. Soc. Lond. 161 (4), 685–693.
Mattioli, E., Pittet, B., Suan, G., Mailliot, S., 2008. Calcareous nannoplankton changes across the early Toarcian oceanic anoxic event in the western Tethys. Paleoceanography 23, PA3208.
McArthur, J.M., 2019. Early Toarcian black shales: a response to an oceanic anoxic event or anoxia in marginal basins? Chem. Geol. 522, 71–83.
McArthur, J.M., Algeo, T.J., van de Schootbrugge, B., Li, Q., Howarth, R.J., 2008. Basinal restriction, black shales, Re-Os dating, and the early Toarcian (Jurassic) oceanic anoxic event. Paleoceanography 23 (4), PA4217.
McElwain, J.C., Wade-Murphy, J., Hesselbo, S.P., 2005. Changes in carbon dioxide during an oceanic anoxic event linked to intrusion into Gondwana coals. Nature 435, 479–495.
Menini, A., Mattioli, E., Hesselbo, S.P., Ruhl, M., Suan, G., 2021. Primary v. carbonate production in the Toarcian, a case study from the Llanbedr (Mochras Farm) borehole, Wales. Geol. Soc. Lond. Spec. Publ. 514, 59–81.
Monaco, P., 1992. Hummocky cross-stratified deposits and turbidites in some sequences of the Umbria-Marche area (Central Italy) during the Toarcian. Sediment. Geol. 77, 123–142.
Monaco, P., 2016. Ichnocoenoses and taphocoenoses of posidoniid-bearing marl-limestone rhythmites and event beds, Toarcian-Aalenian, Northern Apennines, Italy. Geobios 49 (5), 365–379.
Monaco, P., Nocchi, M., Ortega-Huertas, M., Palomo, I., Martinez, F., Chiavini, G., 1994. Depositional trends in the Valdorbia section (Central Italy) during the early Jurassic, as revealed by micropaleontology, sedimentology and geochemistry. Eclogae Geol. Helv. 87, 157–223.
Montero-Serrano, J.C., Föllmi, K.B., Adatte, T., Spangenberg, J.E., Tribovillard, N., Fantasia, A., Suan, G., 2015. Continental weathering and redox conditions during the early Toarcian Oceanic Anoxic Event in the northwestern Tethys: insight from the Posidonia Shale section in the Swiss Jura Mountains. Palaeogeogr. Palaeoclimatol. Palaeoecol. 429, 83–99.
Morettini, E., 1998. Lower Jurassic Stable Isotope Stratigraphy (Carbon, Oxygen, Nitrogen) of the Mediterranean Tethys (Central Italy and Southern Spain). Unpublihsed PhD thesis. Universite´ de Lausanne.
Morton, N., Hudson, J.D., 1995. Field guide to the Jurassic of the Isles of Raasay and Skye, Inner Hebrides, NW Scotland. In: Taylor, P.D. (Ed.), Field Geology of the British Jurassic. Geological Society of London, 209–280 pp.
Müller, T., Karancz, S., Mattioli, E., Milovský, R., Pálfy, J., Schlögl, J., Segit, T., Šimo, V., Tomašových, A., 2020. Assessing anoxia, recovery and carbonate production setback in a hemipelagic Tethyan basin during the Toarcian Oceanic Anoxic Event (Western Carpathians). Glob. Planet. Chang. 195, 103366.
Myhre, G., Alterskjær, K., Stjern, C.W., Hodnebrog, Ø., Marelle, L., Samset, B.H., Sillmann, J., Schaller, N., Fischer, E., Schulz, M., Stohl, A., 2019. Frequency of extreme precipitation increases extensively with event rareness under global warming. Sci. Rep. 9, 16063.
Neumeister, S., Gratzer, R., Algeo, T.J., Bechtel, A., Gawlick, H.J., Newton, R.J., Sachsenhofer, R.F., 2015. Oceanic response to Pliensbachian and Toarcian magmatic events: Implications from an organic-rich basinal succession in the NW Tethys. Glob. Planet. Chang. 126, 62–83.
Nie, Y., Fu, X., Liang, J., Wei, H., Chen, Z., Lin, F., Zeng, S., Wu, Y., Zou, Y., Mansour, A., 2023. The Toarcian Oceanic Anoxic Event in a shelf environment (Eastern Tethys): Implications for weathering and redox conditions. Sediment. Geol. 455, 106476.
Nikitenko, B.L., Reolid, M., Glinskikh, L., 2013. Ecostratigraphy of benthic foraminifera for interpreting Arctic record of early Toarcian biotic crisis (Northern Siberia, Russia). Palaeogeogr. Palaeoclimatol. Palaeoecol. 376, 200–212.
Nordt, L., Breecker, D., White, J., 2022. Jurassic greenhouse ice-sheet fluctuations sensitive to atmospheric $CO_2$ dynamics. Nat. Geosci. 15, 54–59.
Ogg, J.G., Ogg, G.M., Gradstein, F.M., 2016. A concise geological timescale, 80. Elsevier. https://doi.org/10.1016/B978-0-444-59467-9.00012-1.
Osleger, D.A., Heyvaert, A.C., Stoner, J.S., Verosub, K.L., 2009. Lacustrine turbidites as indicators of Holocene storminess and climate: Lake Tahoe, California and Nevada. J. Paleolimnol. 42, 103–122.
Pálfy, J., Smith, P.L., 2000. Synchrony between early Jurassic extinction, oceanic anoxic event, and the Karoo-Ferrar flood basalt volcanism. Geology 28, 747–750.
Palomo Delgado, L., Ortega Huertas, M., Fennol Hach-Ali, P., 1985. The significance of clay minerals in studies of the evolution of the Jurassic deposits of the Betic Cordillera, SE Spain. Clay Miner. 20, 39–52.
Penman, D.E., Caves Rugenstein, J.K., Ibarra, D.E., Winnick, M.J., 2020. Silicate weathering as a feedback and forcing in Earth's climate and carbon cycle. Earth Sci. Rev. 209, 103298.
Percival, L.M.E., Cohen, A.S., Davies, M.K., Hesselbo, S.P., Jenkyns, H.C., Leng, M.J., Mather, T.A., Storm, M.S., Xu, W., 2016. Osmium isotope evidence for two pulses of increased continental weathering linked to early Jurassic volcanism and climate change. Geology 44, 759–762.
Peyser, C.E., Poulsen, C.J., 2008. Controls on Permo-Carboniferous precipitation over tropical Pangaea: a GCM sensitivity study. Palaeogeogr. Palaeocl. 268, 181–192.
Piazza, V., Ullmann, C.V., Aberhan, M., 2020. Temperature-related body size change of marine benthic macroinvertebrates across the early Toarcian Anoxic Event. Sci. Rep. 10, 4675. https://doi.org/10.1038/s41598-020-61393-5.
Pieńkowski, G., Hodbod, M., Ullmann, C.V., 2016. Fungal decomposition of terrestrial organic matter accelerated early Jurassic climate warming. Sci. Rep. 6, 31930.
Pittet, B., Suan, G., Lenoir, F., Duarte, L.V., Mattioli, E., 2014. Carbon isotope evidence for sedimentary discontinuities in the lower Toarcian of the Lusitanian Basin (Portugal): Sea level change at the onset of the Oceanic Anoxic Event. Sediment. Geol. 303, 1–14.
Porcile, G., Bolla Pittaluga, M., Frascati, A., Sequerios, O.E., 2020. Typhoon-induced megarips as triggers of turbidity currents offshore tropical river deltas. Commun. Earth Environ. 1, 2.
Prauss, M., Riegel, W., 1989. Evidence from phytoplankton associations for causes of black-shale formation in epicontinental seas. Neues Jb. Geol. Paläontol. Monat. 11, 671–682.
PSUCLIM, 1999. Storm activity in ancient climates. 2. An analysis using climate simulations and sedimentary structures. J. Geophys. Res. 104 (D22), 27 295–320.
Pujalte, V., Baceta, J.I., Schmitz, B., 2015. A massive input of coarse-grained siliciclastics in the Pyrenean Basin during the PETM: the missing ingredient in a coeval abrupt change in hydrological regime. Clim. Past 11 (12), 1653–1672.
Raucsik, B., Varga, A., 2008. Climato-environmental controls on clay mineralogy of the Hettangian–Bajocian successions of the Mecsek Mountains, Hungary: An evidence for extreme continental weathering during the early Toarcian oceanic anoxic event. Palaeogeogr. Palaeoclimatol. Palaeoecol. 265, 1–13.
Ravizza, G., Norris, R.N., Blusztajn, J., Aubry, M.-P., 2001. An osmium isotope excursion associated with the late Paleocene Thermal Maximum: evidence of intensified chemical weathering. Paleoceanography 16, 155–163.
Remírez, M., Algeo, T.J., 2020. Paleosalinity proxy evidence for watermass restriction in the Cleveland Basin (UK) during the Toarcian OAE. Earth Sci. Rev. 201, 103072.
Reolid, M., Rodríguez-Tovar, F.J., Marok, A., Sebane, A., 2012. The Toarcian oceanic anoxic event in the Western Saharan Atlas, Algeria (North African paleomargin): Role of anoxia and productivity. Geol. Soc. Am. Bull. 124 (9/10), 1646–1664.
Reolid, M., Mattioli, E., Nieto, L.M., Rodríguez-Tovar, F.J., 2014. The early Toarcian oceanic anoxic event in the External Subbetic (Southiberian Palaeomargin, Westernmost Tethys): geochemistry, nannofossils and ichnology. Palaeogeogr. Palaeoclimatol. Palaeoecol. 411, 79–94.
Reolid, M., Abad, I., Benito, I., 2019. Upper Pliensbachian-lower Toarcian methane cold seeps interpreted from geochemical and mineralogical characteristics of celestine concretions (South Iberian palaeo-margin). Palaeogeogr. Palaeoclimatol. Palaeoecol. 530, 15–31.
Reolid, M., Mattioli, E., Duarte, L.V., Marok, A., 2020. The Toarcian Oceanic Anoxic Event and the Jenkyns Event (IGCP-655 final report). Episodes 43 (2), 833–844.
Reolid, M., Soussi, M., Reolid, J., Ruebsam, W., Taher, I.B., Mattioli, E., Saidi, M., Schwark, L., 2021. The onset of the early Toarcian flooding over the Pliensbachian shallow carbonate platform in the North-South Axis (Tunisia): interpretation from trace fossil analysis and geochemistry. Geol. Soc. Lond. Spec. Publ. 514, 213–238.
Roddell, M., Li, B., 2023. Changing intensity of hydroclimatic extreme events revealed by GRACE and GRACE-FO. Nat. Water 1, 241–248.
Rodrigues, B., Duarte, L.V., Mendonça Filho, J.G., Santos, L.G., Donizeti de Oliveira, A., 2016. Evidence of terrestrial organic matter deposition across the early Toarcian recorded in the northern Lusitanian Basin, Portugal. Int. J. Coal Geol. 168, 35–45.
Rodrigues, B., Silva, R.L., Reolid, M., Mendonça Filho, J.G., Duarte, L.V., 2019. Sedimentary organic matter and δ13CKerogen variation on the southern Iberian palaeomargin (Betic Cordillera, SE Spain) during the latest Pliensbachian–Early Toarcian. Palaeogeogr. Palaeoclimatol. Palaeoecol. 534, 109342.
Rodrigues, B., Duarte, L.V., Silva, R.L., Mendonça Filho, J.G., 2020a. Sedimentary organic matter and early Toarcian environmental changes in the Lusitanian Basin (Portugal). Palaeogeogr. Palaeoclimatol. Palaeoecol. 554, 109781.
Rodrigues, B., Silva, R.L., Mendonça Filho, J.G., Comas-Rengifo, M.J., Goy, A., Duarte, L. V., 2020b. Kerogen assemblages and $\delta^{13}C_{Kerogen}$ of the uppermost Pliensbachian–lower Toarcian succession of the Asturian Basin (northern Spain). Int. J. Coal Geol. 229, 103573.
Rodríguez-Tovar, F.J., Uchman, A., 2010. Ichnofabric evidence for the lack of bottom anoxia during the lower Toarcian Oceanic Anoxic Event in the Fuente de la Vidriera section, Betic Cordillera, Spain. Palaios 25, 576–587.
Röhl, H.-J., Schmid-Röhl, A., Oschmann, W., Frimmel, A., Schwark, L., 2001. The Posidonia shale (lower Toarcian) of SW-Germany: an oxygen-depleted ecosystem controlled by sea level and paleoclimate. Palaeogeogr. Palaeoclimatol. Palaeoecol. 169, 273–299.
Rosales, I., Robles, S., Quesada, S., 2004. Elemental and oxygen isotope composition of early Jurassic belemnites: salinity vs. temperature signals. J. Sediment. Res. 74, 343–355.
Rosales, I., Barnolas, A., Goy, A., Sevillano, A., Armendáriz, M., López-García, J.M., 2018. Isotope records (C-O-Sr) of late Pliensbachian-early Toarcian environmental perturbations in the westernmost Tethys (Majorca Island, Spain). Palaeogeogr. Palaeoclimatol. Palaeoecol. 497, 168–185.
Ruebsam, W., Schwark, L., 2024. Disparity between Toarcian Oceanic Anoxic Event and Toarcian carbon isotope excursion. Int. J. Earth Sci. https://doi.org/10.1007/s00531-024-02408-8.
Ruebsam, W., Muenzberger, P., Schwark, L., 2014. Chronology of the early Toarcian environmental crisis in the Lorraine Sub-basin (NE Paris Basin). Earth Planet. Sci. Lett. 404, 273–282.
Ruebsam, W., Müller, T., Kovács, J., Pálfy, J., Schwark, L., 2018. Environmental response to the early Toarcian carbon cycle and climate perturbations in the northeastern part of the West Tethys shelf. Gondwana Res. 59, 144–158.
Ruebsam, W., Mayer, B., Schwark, L., 2019. Cryosphere carbon dynamics control early Toarcian global warming and sea level evolution. Glob. Planet. Chang. 172, 440–453.

Ruebsam, W., Reolid, M., Sabatino, N., Masetti, D., Schwark, L., 2020a. Molecular paleothermometry of the early Toarcian climate perturbation. Glob. Planet. Chang. 195, 103351.
Ruebsam, W., Reolid, M., Schwark, L., 2020b. δ13C of terrestrial vegetation records Toarcian $CO_2$ and climate gradients. Sci. Rep. 10, 117.
Ruebsam, W., Reolid, M., Mattioli, E., Schwark, L., 2021. Organic carbon accumulation at the northern Gondwana paleomargin (Tunisia) during the Toarcian Oceanic Anoxic Event: Sedimentological and geochemical evidence. Palaeogeogr. Palaeoclimatol. Palaeoecol. 586, 110781.
Sabatino, N., Neri, R., Bellanca, A., Jenkyns, H.C., Baudin, F., Parisi, G., Masetti, D., 2009. Carbon isotope records of the early Jurassic (Toarcian) oceanic anoxic event from the Valdorbia (Umbria-Marche Apennines) and Monte Mangart (Julian Alps) sections: palaeoceanographic and stratigraphic implications. Sedimentology 56, 1307–1328.
Sabatino, N., Vlahović, I., Jenkyns, H.C., Scopelliti, G., Neri, R., Prtoljan, B., Velić, I., 2013. Carbon-isotope record and palaeoenvironmental changes during the early Toarcian oceanic anoxic event in shallow-marine carbonates of the Adriatic Carbonate Platform in Croatia. Geol. Mag. 150 (6), 1085–1102.
Schieber, J., Southard, J.B., Schimmelmann, A., 2010. Lenticular shale fabrics resulting from intermittent erosion of water-rich muds – interpreting the rock record in the light of recent flume experiments. J. Sediment. Res. 80, 119–128.
Schmid-Röhl, A., Röhl, H.J., Oschmann, W., Frimmel, A., Schwark, L., 2002. Palaeoenvironmental reconstruction of lower Toarcian epicontinental black shales (Posidonia Shale, SW Germany): global versus regional control. Geobios 35 (1), 13–20.
Sheldon, N.D., 2006. Abrupt chemical weathering increase across the Permian–Triassic boundary. Palaeogeogr. Palaeoclimatol. Palaeoecol. 231, 315–321.
Silva, R.L., Carlisle, C.A.M., Wach, G., 2017. A new TOC, Rock-Eval, and carbon isotope record of lower Jurassic source rocks from the Slyne Basin, offshore Ireland. Mar. Pet. Geol. 86, 499–511.
Simms, M.J., Ruffell, A.H., 1989. Synchroneity of climatic change and extinctions in the late Triassic. Geology 17, 265–268.
Slater, S.M., Twitchett, R.J., Danise, S., Vajda, V., 2019. Substantial vegetation response to early Jurassic global warming with impacts on oceanic anoxia. Nat. Geosci. 12, 462–467.
Steinthorsdottir, M., Vajda, V., 2015. Early Jurassic (late Pliensbachian) $CO_2$ concentrations based on stomatal analysis of fossil conifer leaves from eastern Australia. Gondwana Res. 107, 932–939.
Storm, M.S., Hesselbo, S.P., Jenkyns, H.C., Ruhl, M., Ullmann, C.V., Xu, W., Leng, M.J., Riding, J.B., Gorbanenko, O., 2020. Orbital pacing and secular evolution of the early Jurassic carbon cycle. Proc. Natl. Acad. Sci. 117, 3974–3982.
Studholme, J., Fedorov, A.V., Gulev, S.K., Emanuel, K., Hodges, K., 2021. Poleward expansion of tropical cyclone latitudes in warming climates. Nat. Geosci. 15, 14–28.
Suan, G., Pittet, B., Bour, I., Mattioli, E., Duarte, L.V., Mailliot, S., 2008. Duration of the early Toarcian carbon isotope excursion deduced from spectral analysis: consequence for its possible causes. Earth Planet. Sci. Lett. 267 (3–4), 666–679.
Suan, G., Nikitenko, B.L., Rogov, M.A., Baudin, F., Spangenberg, J.E., Knyazev, V.G., Glinskikh, L.A., Goryacheva, A.A., Adatte, T., Riding, J.B., Föllmi, K.B., Pittet, B., Mattioli, E., Lécuver, C., 2011. Polar record of early Jurassic massive carbon injection. Earth Planet. Sci. Lett. 312 (1–2), 102–113.
Suan, G., Rulleau, L., Mattioli, E., Sucheras-Marx, B., Rousselle, B., Pittet, B., Vincent, P., Martin, J., Léna, A., Spangenberg, J., Föllmi, K.B., 2013. Palaeoenvironmental significance of Toarcian black shales and event deposits from southern Beaujolais, France. Geol. Mag. 150 (4), 728–742.
Suan, G., van de Schootbrugge, B., Adatte, T., Fiebig, J., Oschmann, W., 2015. Calibrating the magnitude of the Toarcian carbon cycle perturbation. Paleoceanography 30, 495–509.
Suan, G., Schlögl, J., Mattioli, E., 2016. Bio- and chemostratigraphy of the Toarcian organic-rich deposits of some key successions of the Alpine Tethys. Newsl. Stratigr. 49 (3), 401–419.
Suan, G., Schöllhorn, I., Schlögl, J., Segit, T., Mattioli, E., Lécuyer, C., Fourel, F., 2018. Euxinic conditions and high sulfur burial near the European shelf margin (Pieniny Klippen Belt, Slovakia) during the Toarcian oceanic anoxic event. Glob. Planet. Chang. 170, 246–259.
Svensen, H., Planke, S., Chevallier, L., Malthe-Sørenssen, A., Corfu, F., Jamtveit, B., 2007. Hydrothermal venting of greenhouse gases triggering early Jurassic global warming. Earth Planet. Sci. Lett. 256, 554–566.
Syvitski, J., Milliman, J.D., 2007. Geology, geography, and humans battle for dominance over the delivery of fluvial sediment to the coastal ocean. J. Geol. 115, 1–19.
Syvitski, J., Restrepo Ángel, J., Saito, Y., Overeem, I., Vörösmarty, C.J., Wang, H., Olago, D., 2022. Earth's sediment cycle in the Anthropocene. Nat. Rev. Earth Environ. 3, 179–196.
Them, T.R., Gill, B.C., Selby, D., Gröcke, D.R., Friedman, R.M., Owens, J.D., 2017a. Evidence for rapid weathering response to climatic warming during the Toarcian Oceanic Anoxic Event. Sci. Rep. 7, 5003.
Them, T.R., Gill, B.C., Caruthers, A.H., Gröcke, D.R., Tulsky, E.T., Martindale, R.C., Poulton, T.P., Smith, P.L., 2017b. High-resolution carbon isotope records of the Toarcian Oceanic Anoxic Event (early Jurassic) from North America and implications for the global drivers of the Toarcian carbon cycle. Earth Planet. Sci. Lett. 459, 118–126.
Them, T.R., Gill, B.C., Caruthers, A.H., Gerhardt, A.M., Gröcke, D.R., Lyons, T.W., Marroquín, S.M., Nielsen, S.G., Trabucho Alexandre, J.P., Owens, J.D., 2018. Thallium isotopes reveal protracted anoxia during the Toarcian (early Jurassic) associated with volcanism, carbon burial, and mass extinction. Proc. Natl. Acad. Sci. 115 (26), 6596–6601.
Thibault, N., Ruhl, M., Ullmann, C.V., Korte, C., Kemp, D.B., Gröcke, D.R., Hesselbo, S.P., 2018. The wider context of the lower Jurassic Toarcian oceanic anoxic event in Yorkshire coastal outcrops, UK. Proc. Geol. Assoc. 129 (3), 372–391.
Trabucho-Alexandre, J., Dirkx, J., Veld, H., Klaver, G., de Boer, P.L., 2012. Toarcian black shales in the Dutch central graben: Record of energetic, variable depositional conditions during an oceanic anoxic event. J. Sediment. Res. 82, 104–120.
Trabucho-Alexandre, J.P., Gröcke, D.R., Atar, E., Herringshaw, L., Jarvis, I., 2023. A new subsurface record of the Pliensbachian–Toarcian, Lower Jurassic, of Yorkshire. Proc. Yorks. Geol. Soc. 64 pygs2022-007.
Trecalli, A., Spangenberg, J., Adatte, T., Föllmi, K.B., Parente, M., 2012. Carbonate platform evidence of ocean acidification at the onset of the early Toarcian oceanic anoxic event. Earth Planet. Sci. Lett. 357, 214–225.
Trenberth, K.E., Dai, A., Rasmussen, R.M., Parsons, D.B., 2003. The changing character of precipitation. Bull. Am. Meteorol. Soc. 84, 1205–1217.
Ullmann, C., Boyle, R., Duarte, L., Hesselbo, S.P., Kasemann, S.A., Klein, T.M., Lenton, T. M., Piazza, V., Aberhan, M., 2020. Warm afterglow from the Toarcian Oceanic Anoxic Event drives the success of deep-adapted brachiopods. Sci. Rep. 10, 6549.
Ullmann, C.V., Szűcs, D., Jiang, M., Hudson, A.J.L., Hesselbo, S.P., 2021. Geochemistry of macrofossil, bulk rock and secondary calcite in the Early Jurassic strata of the Llanbedr (Mochras Farm) drill core, Cardigan Bay Basin, Wales, UK. J. Geol. Soc. Lond. 179 (1) jgs2021-018.
Vakhrameyev, V.A., 1991. Jurassic and Cretaceous Floras and Climates of the Earth. Cambridge University Press, Cambridge, pp. 340–pp.
van Breugel, Y., Baas, M., Schouten, S., Mattioli, E., Sinninghe Damsté, J.S., 2006. Isorenieratane record in black shales from the Paris Basin, France: Constraints on recycling of respired CO2 as a mechanism for negative carbon isotope shifts during the Toarcian oceanic anoxic event. Paleoceanography 21 (4), PA4220.
van de Schootbrugge, B., Bailey, T.R., Rosenthal, Y., Katz, M.E., Wright, J.D., Miller, K. G., Falkowski, P.G., 2005. Early Jurassic climate change and the radiation of organic walled phytoplankton in the Tethys Ocean. Paleobiology 31 (1), 73–97.
van de Schootbrugge, B., Richoz, S., Pross, J., Luppold, F.W., Hunze, S., Wonik, T., Blau, T., Meister, C., van der Weijst, C.M.H., Suan, G., Fraguas, A., Fiebig, J., Herrle, J.O., Guex, J., Little, C.T.S., Wignall, P.B., Püttmann, W., Oschmann, W., 2018. The Schandelah Scientific Drilling Project: a 25-million year record of early Jurassic palaeo-environmental change from northern Germany. Newsl. Stratigr. 52 (3), 249–296.
van de Schootbrugge, B., Houben, A.J.P., Ercan, F.E.Z., Verreussel, R., Kerstholt, S., Janssen, N.M.M., Nikitenko, B., Suan, G., 2019. Enhanced Arctic-Tethys connectivity ended the Toarcian Oceanic Anoxic Event in NW Europe. Geol. Mag. 157, 1593–1611.
Walker, J.G.C., Hays, P.B., Kasting, J.F., 1981. A negative feedback mechanism for the long-term stabilization of Earth's surface temperature. J. Geophys. Res. Oceans 86, 9776–9782.
Wei, W., Algeo, T.J., 2019. Elemental proxies for paleosalinity analysis. Geochim. Cosmochim. Acta 287, 341–366.
Wignall, P.B., Newton, R.J., Little, C.T., 2005. The timing of paleoenvironmental change and cause-and-effect relationships during the early Jurassic mass extinction in Europe. Am. J. Sci. 305 (10), 1014–1032.
Woodfine, R.G., Jenkyns, H.C., Sarti, M., Baroncini, F., Violante, C., 2008. The response of two Tethyan carbonate platforms to the early Toarcian (Jurassic) oceanic anoxic event: environmental change and differential subsidence. Sedimentology 55, 1011–1028.
Wright, V.P., Wilson, R.C.L., 1984. A carbonate submarine fan sequence from the Jurassic of Portugal. J. Sediment. Petrol. 54, 394–412.
Xia, G., Mansour, A., Gentzis, T., Li, G., Carvajal-Ortiz, H., Ocubaliedet, S., Yi, F., Yun, C., Yi, H., 2021. Depositional paleoenvironment and source rock characterization across the Toarcian oceanic anoxic event from the eastern Tethys, Tibet, SW China. Int. J. Coal Geol. 243, 103780.
Xu, W., Ruhl, M., Jenkyns, H., Hesselbo, S., Riding, J., Selby, D., Naafs, B., Weijers, J., Pancost, R., Tegelaar, E., 2017. Carbon sequestration in an expanding lake system during the Toarcian Oceanic Anoxic Event. Nat. Geosci. 10, 129–135.
Xu, W., Ruhl, M., Jenkyns, H.C., Leng, M.J., Huggett, J.M., Minisini, D., Ullmann, C., Riding, J., Weijers, J., Storm, M., Percival, L., Tosca, N., Idiz, E.F., Tegelaar, E.W., Hesselbo, S.P., 2018. Evolution of the Toarcian (early Jurassic) carbon-cycle and global climatic controls on local sedimentary processes (Cardigan Bay Basin, UK). Earth Planet. Sci. Lett. 484, 396–411.
Xu, W., Weijers, J.W.H., Ruhl, M., Idiz, E.F., Jenkyns, H.C., Riding, J.B., Gorbanenko, O., Hesselbo, S.P., 2021. Molecular and petrographical evidence for lacustrine environmental and biotic change in the palaeo-Sichuan megalake (China) during the Toarcian Oceanic Anoxic Event. Geol. Soc. Lond. Spec. Publ. 514, 335–357.
Yan, Q., Li, X., Kemp, D.B., Guo, J., Zhang, Z., Hu, Y., 2023. Elevated atmospheric CO2 drove an increase in tropical cyclone intensity during the early Toarcian hyperthermal. PNAS 120 (29), e2301018120.
Yang, J., Cawood, P., Yuan, X., Yuan, D., Zhou, Y., Liu, A., Liu, J., Du, Y., 2023. Enhanced denudation of the Emeishan large Igneous Province and precipitation forcing in the late Permian. J. Geophys. Res. Solid Earth 128 (12), e2023JB027430.
Yi, J.Q., Fu, X.G., Du, Q.D., Wei, H.Y., Mansour, A., Nie, Y., Zeng, Y.H., Deng, J.X., Zhou, G., Wang, W.Z., Shen, L.J., 2023. Accelerated hydrological cycle during the Toarcian oceanic anoxic event: biomarker evidence in the Qiangtang Basin, eastern Tethys. J. Asian Earth Sci. 249, 105627.
Zakharov, V., Shurygin, B., Ilyna, V., Nikitenko, B., 2006. Pliensbachian-Toarcian biotic turnover in North Siberia and the Arctic region. Stratigr. Geol. Correl. 14, 399–417.
Zavala, C., Pan, S., 2018. Hyperpycnal flows and hyperpycnites:Origin and distinctive characteristics. Lithol. Reserv. 30 (1), 1–27.